Evaluating Coarse-Grained MARTINI Force-Fields for Capturing the Ripple Phase of Lipid Membranes

***Pradyumn Sharma*[1,‡], *Rajat Desikan*[1,‡,†], *K. Ganapathy Ayappa*[1,2,*]**

[1]Department of Chemical Engineering, Indian Institute of Science, Bengaluru, India

[2]Centre for BioSystems Science and Engineering, Indian Institute of Science, Bengaluru, India

[‡]Co-first authors

[†]Present address: Certara QSP, Certara UK Limited, Sheffield, UK

*Corresponding author: K. Ganapathy Ayappa; E-mail: ayappa@iisc.ac.in

Manuscript details:

Title: 96 characters (with spaces); Abstract: 298 words; Figures: 6; Tables: 2; References: 78; Supporting figures: 13

Keywords:

Molecular dynamics; multiscale simulations; CHARMM36; MARTINI; lipid membrane; DPPC; tilted ripple phase; gel phase; phase transition

Abstract

Phospholipids, which are an integral component of cell membranes, exhibit a rich variety of lamellar phases modulated by temperature and composition. Molecular dynamics (MD) simulations have greatly enhanced our understanding of phospholipid membranes by capturing experimentally observed phases and phase transitions at molecular resolution. However, the ripple ($P_{\beta'}$) membrane phase, observed as an intermediate phase below the main gel-to-liquid crystalline transition with some lipids, has been challenging to capture with MD simulations, both at all-atom and coarse-grained (CG) resolution. Here, with an aggregate ~2.5 μs all-atom and ~122 μs CG MD simulations, we systematically assess the ability of six CG MARTINI 1,2-dipalmitoyl-sn-glycero-3-phosphocholine (DPPC) lipid and water force-field (FF) variants, parametrized to capture the DPPC gel and fluid phases, for their ability to capture the $P_{\beta'}$ phase, and compared observations with those from an all-atom FF. Upon cooling from the fluid phase to below the phase transition temperature with smaller (380-lipid) and larger (> 2200-lipid) MARTINI and all-atom (CHARMM36 FF) DPPC lipid bilayers, we observed that smaller bilayers with both all-atom and MARTINI FFs sampled interdigitated $P_{\beta'}$ and ripple-like states, respectively. However, while all-atom simulations of the larger DPPC membranes exhibited the formation of the $P_{\beta'}$ phase, similar to previous studies, MARTINI membranes did not sample interdigitated ripple-like states at larger system sizes. We then demonstrated that the ripple-like states in smaller MARTINI membranes were kinetically-trapped structures caused by finite size effects rather than being representative of true $P_{\beta'}$ phases. We showed that even a MARTINI FF variant that could capture the tilted $L_{\beta'}$ gel phase, a prerequisite for stabilizing the $P_{\beta'}$ phase, could not capture the rippled phase upon cooling. Our study reveals that the current MARTINI FFs (including MARTINI3) may require specific re-parametrization of the interaction potentials to stabilize lipid interdigitation, a characteristic of the ripple phase.

45 ## Introduction

46 Lamellar lipid membranes, composed of two layers of amphiphilic lipids with solvated
47 hydrophilic 'heads' and buried hydrophobic 'tails', exhibit a wide variety of thermotropic phases
48 such as crystalline (L_c), tilted gel ($L_{\beta'}$) or straight gel (L_β), tilted ripple ($P_{\beta'}$), and liquid-crystalline
49 (L_α).[1,2] Lipid bilayers are important constituents of biomembranes which are ubiquitous in living
50 organisms[3], and nanoparticle pharmaceuticals such liposomal drugs[4–6]. Specifically, lipid
51 membrane phases influence: (i) biological processes at the cellular level such as membrane
52 fusion and budding[7], permeation of drugs[8,9], effect of anaesthetics[10], vulnerability to pathogenic
53 toxins[11,12], lipid flip-flop[13,14], neural signalling[15], and the function of membrane proteins[3,7], and (ii)
54 industrial applications such as the design, storage and usage of liposomal drugs[4–6,16], cosmetic
55 formulations[1], and lipid-rich foods[1]. Molecular simulations of membranes at various levels of detail
56 have yielded atomistic insights into the rich phase behaviour of phospholipid membranes while
57 complementing experimental observations[1,17]. All-atom molecular dynamics (MD) simulations
58 have successfully captured the low temperature $L_{\beta'}$ or L_β phases, the liquid ordered and liquid
59 disordered phases, and the main gel-to-fluid ($L_{\beta'}$ to L_α) phase transition in simple lipid bilayers
60 while providing detailed insights into the rate-limiting formation of the melting seed that nucleates
61 the transition[18]. Similarly, the molecular structure of lipid domains in the experimentally elusive
62 $P_{\beta'}$ phase, which commonly occurs upon cooling membranes from the L_α phase to below the gel-
63 to-fluid transition temperature (pre-transition region), was unravelled at atomistic resolution via
64 detailed MD simulations[19–21] and was found to be consistent with experimental observations.

65 While these *in silico* studies illustrate the wide applicability of all-atom lipid force-fields
66 (FFs), all-atom MD simulations are typically limited by computational bottlenecks to nanoscales,
67 and complex membrane processes typically require microscale MD simulations[17,22]. Therefore,
68 coarse-grained (CG) lipid models such as those used in the dissipative particle dynamics (DPD),
69 MARTINI, and other frameworks have been developed[22–26]. Among the CG models, the MARTINI

70 biomolecular FF has been successfully used to study a variety of complex biological systems
71 outside the purview of all-atom MD simulations[22]. For example, MARTINI simulations have been
72 used to carry out microsecond simulations of an idealized 20000-lipid plasma membrane
73 comprising 63 different species of lipids[27], a difficult feat with typical all-atom simulations. The
74 MARTINI model is based on a four-to-one mapping scheme where four non-hydrogen atoms are
75 typically modelled as effective CG interaction sites ('beads'), whose parameters were calibrated
76 by comparison with macroscopic properties such as thermodynamic transfer free energies
77 (Details of bead types and FF parameterization in Refs.[22,24,28]). The versatility and computational
78 tractability of CG models such as MARTINI render them as attractive options for capturing the
79 microscopic details of complex membrane phenomena[22,24]. However, since CG models by
80 definition possess reduced molecular detail[28], their interaction potentials must be continuously
81 assessed and refined, often by systematic comparison with experiments and/or corresponding
82 detailed all-atom models[25,26,28–33], to enable increasingly accurate CGMD simulations.

83 DPPC possesses a large headgroup and favourable inter-head interactions that stabilizes
84 a tilted gel ($L_{\beta'}$) phase at lower temperatures, unlike lipids with smaller headgroups such as
85 phosphatidylethanolamine that favour the straight gel (L_{β}) phase[20,21,34]. At higher temperatures,
86 DPPC exhibits a main $L_{\beta'}$ to L_{α} phase transition, with the $P_{\beta'}$ phase occurring at pre-transition
87 temperatures[34–40]. The $P_{\beta'}$ phase has interesting properties such as the influence of thermal
88 history on the symmetry of the ripple domains[20], and therefore has been the subject of extensive
89 experimental[35,39–42] and theoretical[18–21,25,31,37,38,43–47] studies. In Table 1, we summarize some of
90 the previous studies where the rippled phase has been observed, including details of lipid type,
91 resolution (all-atom, united atom or coarse-grained) and FF. Despite extensive *in silico*
92 investigations, MD simulations that capture the $P_{\beta'}$ phase have proven to be challenging since
93 the ripple domain structure and formation is not only a function of the specific lipid FF (Table 1),
94 but also depends on the cooling/heating protocols[18,36] and system size effects[20,36,45]. In spite of
95 these challenges, MD simulations of lipid bilayers in the ripple phase have revealed elusive details

96 of molecular organization that were challenging to probe via experiments, such as the asymmetric
97 sawtooth-like molecular organization of lipids in the DPPC ripple domains[19–21].

98 **Table 1. List of previous studies which have explored the $P_{\beta'}$ phase using MD simulations.**

Lipid	*Year*	*Resolution*	*Force-field*	*Comparison with experiments*	*Citation*
DPPC	2005	United atom	Modified Berger lipid	Qualitative comparison with DMPC electron density profiles	Ref.[19]
DMPC	2005	Coarse-grained	DPD	–	Ref.[21]
DPPC	2007	Coarse-grained	Custom (single tailed)	Qualitative comparison with DPPC electron density maps	Ref.[20]
DMPC, DPPC	2012	Coarse-grained	DPD, MARTINI	Enthalpic signatures of phase transitions from MD compared with differential scanning calorimetry	Ref.[36]
BTMAC+SA	2014	United atom	GROMOS 87, OPLS	–	Ref.[43]
DPPC	2014	Coarse-grained	MARTINI	–	Ref.[48]
DMPC	2016	All-atom	CHARMM36, Lipid14	–	Ref.[44]
DPPC	2017	Coarse-grained	Dry MARTINI	–	Ref.[49]
DMPC, DPPC	2018	All-atom	CHARMM36	Comparison of bilayer properties with X-ray diffraction experiments	Ref.[46]
DPPC	2018	All-atom	CHARMM36	–	Ref.[18]
DPPC	2018	All-atom, coarse-grained	CHARMM36, MARTINI	–	Ref.[31]
DPPC	2019	All-atom	CHARMM36	–	Ref.[45]
BTMAC+SA	2020	All-atom, coarse-grained	CHARMM36, MARTINI	–	Ref.[25]

99 Abbreviations: DPD – dissipative particle dynamics; DPPC – 1,2-dipalmitoyl-sn-glycero-3-phosphocholine; DMPC –
100 1,2-dimyristoyl-sn-glycero-3-phosphocholine; BTMAC – benzyltrimethylammonium chloride; SA – stearyl alcohol.

101 While DPPC membranes described by the standard MARTINI FF and its variants have
102 been shown to capture the gel and fluid states[22,31], there are conflicting reports of their ability to
103 capture the ripple phase. Some MARTINI studies have reported ripple formation both with and
104 without enhanced sampling[31,48,49], while others have reported that MARTINI membranes cannot
105 capture the ripple phase[36], with the interdigitated ripple-like domains observed upon quasi-static

106 cooling from the L_α phase reported to be artefacts caused by finite size effects[36]. Therefore, the
107 ability of MARTINI membranes to capture the $P_{\beta'}$ phase still remains an unresolved problem. To
108 systematically address this issue, we assess the ability of commonly employed[18,19,23,29,31,36,45,46,48]
109 DPPC bilayers, described by six MARTINI lipid FF variants (described subsequently), to capture
110 the interdigitated tilted ripple membrane phase ($P_{\beta'}$).

111 We first establish a standard simulated-annealing-based cooling MD protocol, built on
112 previous studies[18–20,31,45,46], that consistently yielded a ripple phase upon cooling from the fluid
113 phase to below the gel-to-fluid phase transition temperature with all-atom DPPC membranes
114 across multiple simulation replicates. By employing the same protocol with MARTINI DPPC
115 membranes, and by fixing other important variables such as initial configurations (L_α phase),
116 system sizes and cooling rates, we checked whether the MARTINI membranes yielded stable
117 ripple phase structures, similar to those observed in all-atom simulations. Six MARTINI lipid and
118 water FF combinations were tested: (1) standard MARTINI version 2.2 lipid FF with normal water
119 ('MARTINI2n')[23], or polarizable water[50] ('MARTINI2p') with embedded charges and explicit
120 charge screening for better electrostatics[22], (2) optimized MARTINI FF for DPPC – has refined
121 bond parameters for better reproduction of DPPC membrane phase behaviour and can capture
122 the tilted $L_{\beta'}$ gel phase – with either normal ('MARTINI2On') or polarizable ('MARTINI2Op') water,
123 and, (3) the recently released MARTINI 3 alpha ('MARTINI3a')[33], and the slightly different
124 previous interim version MARTINI 3 beta (version 3.0.b.3.2; 'MARTINI3b')[51], with their in-built
125 water models. The next generation MARTINI3 FFs include new parameterization of charged
126 beads as well as small and tiny beads involved in aromatic groups, improved bead interactions,
127 and extensive benchmarking, and MARTINI3a is poised to replace MARTINI2 as the default
128 choice of MARTINI FF[33,51]. For each FF variant, 10 independent replicates of simulated cooling
129 were performed, ensuring sufficient sampling for robust statistical estimates[18,52]. We observed
130 that smaller (380-lipid) MARTINI DPPC bilayers sampled interdigitated ripple-like states that were
131 not observed with larger DPPC membranes (> 2200-lipid). The ripple-like states in these smaller

132 MARTINI DPPC membranes were demonstrated to be kinetically-trapped structures caused due
133 to finite size effects, rather than being representative of a true ripple phase. However, all-atom
134 simulations of both the smaller and larger DPPC membranes exhibited the formation of the $P_{\beta'}$
135 phase, similar to previous studies. Our observations thus assess the ability of MARTINI lipid FFs
136 to capture the ripple phase and serve as a guide for future CG lipid FF development.

137

138 ## Methods

139 **All-atom MD simulations of DPPC membranes**

140 The MD protocols employed in this study for simulating DPPC membranes in the gel, ripple
141 and fluid phases are briefly described below. All the simulations performed in this study are
142 summarized in Table 2.

143 For the small membrane atomistic simulations, two charge-neutral, solvated, fluid phase
144 (L_α), 368-lipid membrane configurations at 350 K, with similar spatial coordinates but different
145 starting velocities, were set up using CHARMM-GUI[53–55] as independent replicates (Figures 1
146 and S1). The size of the lipid patches was approximately 15.2 nm (x-axis) x 7.6 nm (y-axis) x 9.4
147 nm (z-axis), with the characteristic dimension of the simulation box in the membrane plane in the
148 range of the periodicity of 12-16 nm corresponding to previously observed ripple profiles in DPPC
149 membranes[19,56]. This was important because the quality of the observed ripples was found to
150 depend on the characteristic box dimension along the ripple formation[20]. Systems whose
151 characteristic box length in the membrane plane were non-integer multiples of ripple periodicity
152 resulted in frustrated and interconnected structures, unlike the clean ripples observed in systems
153 with integer multiple box lengths[20]. Each system contained >10^5 atoms. The water:lipid ratio was
154 set at 50:1, ensuring sufficient hydration normal to the membrane plane (z), so that the systems
155 could be approximated as isolated lipid bilayers along the z-axis.

156 Atomistic simulations were performed using the CHARMM36 FF[44,57,58] implementation
157 (March 2019 version from http://mackerell.umaryland.edu/charmm_ff.shtml) in Gromacs (version
158 2018.6)[59], according to the currently advocated best practices for lipid bilayer simulations[17,60–62].
159 (See Refs.[30,44] for a brief discussion of all-atom and united atom lipid FFs.) A leapfrog integrator
160 (2 fs integration time step) was used along with Verlet buffered lists and three-dimensional
161 periodic boundary conditions. Electrostatic interactions were computed with the particle mesh
162 Ewald algorithm[63], and van der Waal interactions were smoothly switched to zero between 1.0 to
163 1.2 nm. Covalent bonds involving hydrogen atoms were constrained using the LINCS algorithm[64].
164 Simulations were performed in the NPT ensemble with semi-isotropic pressure coupling along
165 the lateral bilayer plane, by employing the stochastic velocity-rescaling thermostat[65] for
166 temperature control, and the Parrinello-Rahman barostat[66] for pressure control, with coupling
167 constants of 0.1 and 2.0 ps, respectively. The isothermal compressibilities for the barostat were
168 $\kappa_{XY} = \kappa_Z = 4.5 \times 10^{-5}$ bar^{-1}. After energy minimization and equilibration (100 ns) of the initial
169 configurations in the L_α phase (350 K) according to standard CHARMM-GUI protocols[54], the
170 systemic temperatures of the replicates were continuously reduced from 350 K to 290 K at the
171 rate of 1 K per 6 ns, or -0.167 K/ns, by employing the stochastic simulated annealing MD (SAMD)
172 algorithm implemented in Gromacs[59] (360 ns per SAMD replicate). We chose to cool slightly
173 beyond the pre-transition temperature of 300-310 K at which the $P_{\beta'}$ phase is typically
174 observed[18,34,36–38], because super-cooling is often required in kinetic MD simulations for eliciting
175 a phase transition[18,67,68]. The resulting cooled bilayers at 290 K were further equilibrated at a
176 constant temperature of 290 K for 200 ns for thermal and structural stability.

177 To test for finite size effects and to compare with MARTINI simulations (described next),
178 two large 2208-lipid membranes measuring 47.0 nm x 15.7 nm x 15.0 nm and possessing a high
179 water:lipid ratio of 128:1 (>10^6 atoms total; Table 2) were equilibrated in the L_α phase at 350 K.
180 Subsequently, both replicates were cooled to 290 K at the rate of -0.167 K/ns (chosen based on
181 Ref.[18]) and then equilibrated at 290 K for an additional 200 ns.

182 **MARTINI simulations of DPPC membranes**

183 380-lipid MARTINI DPPC membranes of size 15 nm x 7.5 nm x 10 nm were prepared using
184 the 'INSANE' python module[69]. The water-bead:lipid ratio was ~13.3:1. Since each water bead is
185 equivalent to 4 water molecules, this corresponds to a water:lipid ratio of ~53:1, similar to the
186 small all-atom membranes. As described in the Introduction, six MARTINI FF variants were used
187 in this study: MARTINI2n[23], MARTINI2p[50], MARTINI2On[31], MARTINI2Op[31,50], MARTINI3a[33], and
188 MARTINI3b[51]. MARTINI2n and MARTINI2On systems also contained anti-freeze solvent beads[23]
189 to prevent any artefactual freezing of MARTINI water beads.

190 Input CGMD parameters were fixed based on previously reported parameter settings for
191 improved performance[70]. All CGMD simulations were performed with a 20 fs timestep in the NPT
192 ensemble by employing the stochastic velocity-rescaling thermostat[65] (coupling constant of 1.0
193 ps) and the Parrinello-Rahman semi-isotropic barostat[66] (coupling constant of 12.0 ps). The
194 isothermal compressibilities for the barostat were $\kappa_{XY} = \kappa_Z = 3 \times 10^{-4}$ bar^{-1}. Electrostatics were
195 treated with the reaction-field algorithm[71] with a cut-off of 1.1 nm, relative dielectric constant of
196 2.5 and 15 for systems with and without polarizable water, respectively, and the relative dielectric
197 constant of the reaction field set to infinity. The van der Waal forces were computed with a cut-off
198 of 1.1 nm. Post energy minimization, six CGMD membranes, each described by a MARTINI FF
199 variant, were equilibrated in the L_α phase at 350 K for 100 ns, followed by simulated cooling from
200 350 K to 280 K at -0.167 K/ns (420 ns per SAMD replicate). For each FF, 10 independent SAMD
201 replicates were simulated for ensuring robustness of observations[52], resulting in a total of 60 CG-
202 SAMD simulations (Figures 2, S2-S7). The replicates which yielded the best ripple-like phases
203 were further equilibrated for 1-5 μs at 280 K to ensure that the ripples had attained thermal and
204 structural equilibrium (Figures 2 and S5*b*).

205 To test for finite-size effects, many large MARTINI DPPC bilayer configurations, with both
206 rectangular and square geometries, were constructed and simulated (Table 2).

Table 2. Summary of all-atom and MARTINI simulations performed in this study.

Forcefield	*Time (μs)*[#]	*Number of replicas*	*System size (L_x x L_y x L_z nm^3)*	*Number of lipids*	*Number of particles*	*Type of MD simulation*[a]	*Temp. (K)*	*Figures*
Small membrane simulations								
CHARMM36	0.10	1	15.7 x 7.8 x 8.4	368	103040	EQMD[&]	350	1, S1
CHARMM36	0.36	2	13.4 x 6.7 x 10.6	368	103040	SAMD	350-290	
CHARMM36	0.20	2	13.4 x 6.7 x 10.6	368	103040	EQMD	290	
MARTINI2n	0.10	1	15.8 x 7.9 x 9.6	380	9626	EQMD[&]	350	2
MARTINI2On	0.10	1	15.8 x 7.9 x 9.6	380	9620	EQMD[&]	350	-
MARTINI3a	0.10	1	16.1 x 8.0 x 8.8	380	9626	EQMD[&]	350	
MARTINI3b	0.10	1	15.9 x 7.9 x 9.1	380	9626	EQMD[&]	350	-
MARTINI2p	0.10	1	16.0 x 8.0 x 9.0	380	19761	EQMD[&]	350	-
MARTINI2Op	0.10	1	15.5 x 7.8 x 9.5	380	19764	EQMD[&]	350	-
MARTINI2n	0.42	10	14.2 x 7.1 x 11.1	380	9626	SAMD	350-280	S2
MARTINI2On	0.42	10	13.9 x 7.0 x 11.5	380	9620	SAMD	350-280	S3
MARTINI3a	0.42	10	14.1 x 7.1 x 10.5	380	9626	SAMD	350-280	S4
MARTINI3b	0.42	10	14.2 x 7.1 x 10.5	380	9626	SAMD	350-280	S5
MARTINI2p	0.42	10	14.4 x 7.2 x 10.2	380	19761	SAMD	350-280	S6
MARTINI2Op	0.42	10	13.8 x 6.9 x 10.9	380	19764	SAMD	350-280	S7
MARTINI2n	5	2[b]	14.3 x 7.1 x 11.0	380	9626	EQMD	280	2, 6
MARTINI2On	5	3[c]	13.9 x 7.0 x 11.4	380	9620	EQMD	280	2, 6, S13
MARTINI3a	5	1[d]	14.1 x 7.1 x 10.5	380	9626	EQMD	280	2
MARTINI3b	5	1[e]	14.0 x 7.0 x 10.7	380	9626	EQMD	280	S5*b*
MARTINI2p	5	1[f]	14.3 x 7.2 x 10.2	380	19761	EQMD	280	2
MARTINI2Op	5	1[g]	13.8 x 6.9 x 10.9	380	19764	EQMD	280	2
Large membrane simulations								
CHARMM36	0.02	1	46.4 x 15.4 x 16.1	2208	1135872	EQMD[&]	350	3, S8
CHARMM36	0.36	2	40.3 x 13.4 x 19.9	2208	1135872	SAMD	350-290	
CHARMM36	0.20	2	40.4 x 13.5 x 19.8	2208	1135872	EQMD	290	
MARTINI2n	0.10	2	46.5 x 15.5 x 20.6	2204	112719	EQMD[&]	350	4
MARTINI2On	0.10	2	46.3 x 15.4 x 20.8	2204	112719	EQMD[&]	350	-
MARTINI3a	0.10	2	46.6 x 15.5 x 19.1	2204	112717	EQMD[&]	350	-
MARTINI3b	0.10	2	47.1 x 15.7 x 18.8	2204	112717	EQMD[&]	350	-
MARTINI2n	0.42	2	39.9 x 13.3 x 26.0	2204	112719	SAMD	350-280	4, S10
MARTINI2On	0.42	2	39.9 x 13.1 x 26.6	2204	112719	SAMD	350-280	
MARTINI3a	0.42	2	39.3 x 13.1 x 24.9	2204	112717	SAMD	350-280	
MARTINI3b	0.42	2	41.3 x 13.8 x 22.7	2204	112717	SAMD	350-280	
MARTINI2n	3	1	39.6 x 13.2 x 12.7	2280	57756	EQMD	280	5, S12
MARTINI2On	5, 8, 10	3	39.7 x 13.2 x 12.6	2280	57720	EQMD	280	5, 6, S12, S13
MARTINI3a	10	1	39.8 x 13.3 x 11.9	2280	57756	EQMD	280	5, S12
MARTINI3b	10	1	40.0 x 13.3 x 11.8	2280	57756	EQMD	280	S12
MARTINI2On	0.10	1[h]	46.5 x 46.5 x 20.2	6728	333604	EQMD[&]	350	S11
MARTINI2On	0.42	2[h]	39.5 x 39.5 x 26.0	6728	333604	SAMD	350-280	S11

[#]Simulation times from MARTINI CGMD were <u>not</u> scaled. Total simulation time in this study: ~2.5 μs (all-atom MD) and ~122 μs (MARTINI CGMD). [&]Initial simulations to equilibrate starting configurations. [a]EQMD – equilibrium MD simulations in the NPT ensemble; SAMD – simulated annealing MD simulations at constant pressure. [b]Replicates with the 'best' ripple-like (Repl. 1 in Figure S2) and straight gel (Repl. 7 in Figure S2) phases were further equilibrated for 5000 ns. [c]Replicates with the 'best' ripple-like (Repl. 5 in Figure S3), tilted ripple-like (Repl. 7 in Figure S3) and tilted gel (Repl. 3 in Figure S3) phases were further equilibrated for 5000 ns. Replicates with the 'best' ripple-like phase: [d]Repl. 5 in Figure S4, [e]Repl. 9 in Figure S5, [f]Repl. 5 in Figure S6, and [g]Repl. 10 in Figure S7, were further equilibrated for 5000 ns each. [h]Square membrane patch; all others are rectangular membrane patches.

Analysis and visualization

MD snapshots are illustrated using the visual molecular dynamics 1.9.3 (VMD)[72] software. The DPPC tails in the upper and lower leaflets of both all-atom and MARTINI membranes are consistently colored cyan and magenta, respectively. In all-atom membranes, phosphorus atoms (P) are colored orange, and nitrogen atoms in the choline group are colored blue. Similarly, in MARTINI membranes, the phosphate bead is colored orange and the choline bead is colored blue. The minimum inter-leaflet P-P distance (ξ), which is an order parameter to track leaflet interdigitation (Figure 1*b*), was computed using the inbuilt 'gmx mindist' tool in Gromacs. The ξ from the fluid and interdigitated regimes are fit to a four-parameter piecewise-linear function (Equation 1) to accurately estimate the time of the onset of membrane interdigitation, τ.

$$\xi = (m_1 t + c)\big(1 - H(t-\tau)\big) + (m_2 t + (m_1 - m_2)\tau + c)H(t-\tau) \qquad -(1)$$

Here, m_1 and m_2 are the slopes of the two lines corresponding to the fluid and interdigitated regimes (when it occurs), respectively, c is the intercept of the fluid-phase line (the intercept of the other line is $(m_1 - m_2)\tau + c$ from the point of intersection), and $H(t-\tau)$ is the Heaviside function which is zero for $t < \tau$, and one for $t \geq \tau$. If interdigitation occurs, $m_2 < 0$, else $m_2 > 0$ (illustrated in Figure S2). The fitting was performed using the 'lsqcurvefit' function (optimization toolbox) in conjunction with 'multistart' (global optimization toolbox) implemented in MATLAB 2018a (https://www.mathworks.com). All other plots are also created with MATLAB. The combined Voronoi-thickness modulation heatmaps are plotted using the 'voronoi' MATLAB function on the lipid phosphorus atom x, y coordinates (upper leaflet) from the corresponding MD snapshot. The membrane thickness[43] is computed using the 'Membplugin' 1.1 tool[73] in VMD and visualized using MATLAB. Similar to a previous study[74], lipid tilt angles from MARTINI membranes (L_β vs. $L_{\beta'}$) were computed from the last 10 ns of the respective MD trajectories, using the inbuilt 'gmx gangle' tool in Gromacs. The lipid tilt was defined as the angle between the

239 lipid vector and the leaflet normal, with the lipid vector defined as the vector joining the center of
240 mass of the terminal tail beads with the head phosphate bead.

241

242 Results & Discussion

243 Ripple formation in atomistic simulations of DPPC membranes

244 To robustly capture the ripple phase in all-atom DPPC membranes[26], well-equilibrated,
245 fluid, 368-lipid DPPC membranes at 350 K (time point I in Figure 1*a, c*) were cooled to 290 K,
246 lower than the experimentally observed pre-transition temperature of 300-310 K[34,36–38] and
247 sufficient to ensure leaflet interdigitation[18,46], using the stochastic simulated annealing MD
248 algorithm, followed by constant temperature equilibration MD (EQMD) in the NPT ensemble at
249 290 K to ensure thermal equilibration and structural convergence (details in Methods; 2
250 independent MD replicates). Along with the initial state (time point I), three other time points are
251 important in the combined SAMD+EQMD trajectory (Figure 1*a, c*) – the fluid membrane
252 configuration where interdigitation starts (time point II), the fully interdigitated ripple phase
253 membranes at the end of simulated cooling (time point III), and the converged systems at the end
254 of constant temperature equilibration (time point IV). The extent of interdigitation was tracked by
255 the minimum inter-leaflet P-P distance with time (ξ; Methods and Equation 1; Figure 1*b, c*). A
256 higher initial value marked the baseline corresponding to the fluid phase (350 K; time point I), and
257 an abruptly decreasing trend indicated significant interdigitation of lipids from opposite leaflets,
258 with the onset of interdigitation marked by the inflection point (time point II – τ; see Methods,
259 Figure S2, and Equation 1). By the end of simulated cooling (290 K; time point III), interdigitation
260 was complete and a membrane with an 'asymmetric'[20] 1D ripple was formed, similar in structure
261 to previous studies[19,20,45,46], structurally stable upon further 200 ns equilibration at 290 K (time
262 point IV), and with clearly distinct major and minor arms (illustrated in Figure S1*a*).

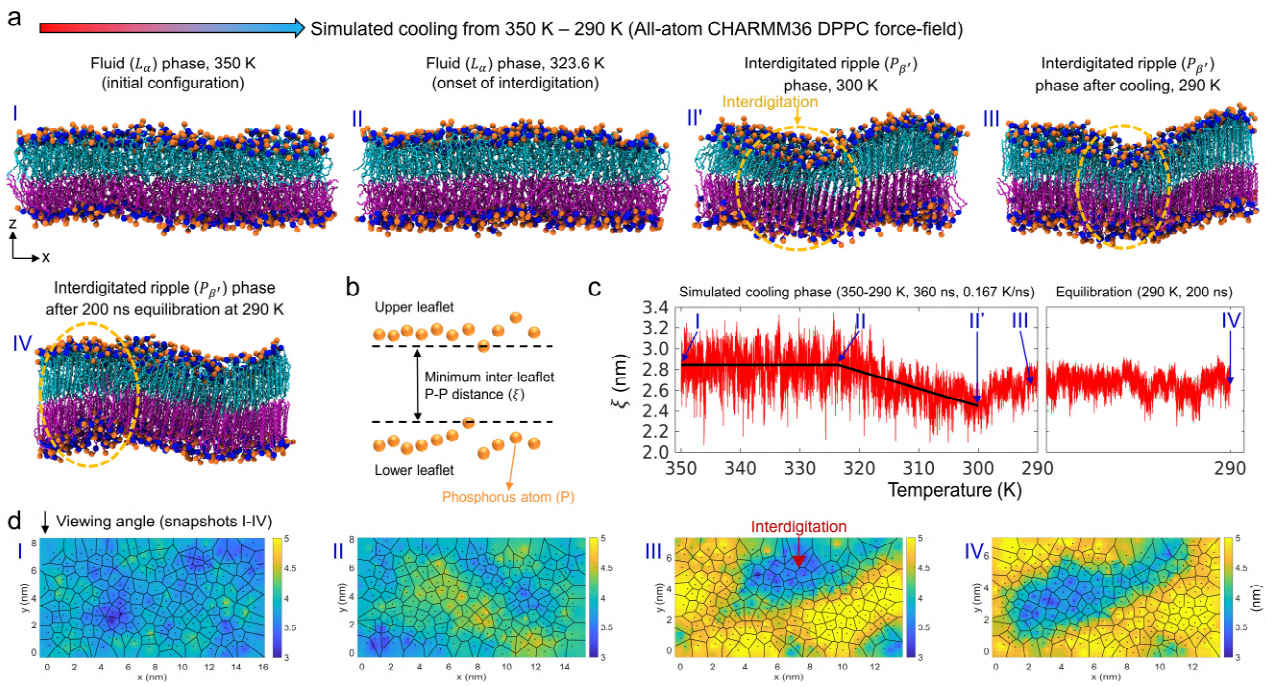

Figure 1. All-atom L_α DPPC membranes consistently form ripples upon cooling. (a) MD snapshots (colouring described in Methods) during the cooling of a 368-lipid, all-atom, DPPC membrane from 350 K to 290 K. Time points: I – initial equilibrated L_α phase membrane at 350 K before the start of cooling, II – start of interdigitation, II' –time at which the average inter-leaflet distance in the time series is at a minimum (300 K), III – end of simulated cooling (290 K), and IV – end of equilibration MD at constant temperature (290 K). Interdigitated domains are highlighted by yellow dashed circles. **(b)** Schematic illustrating the minimum inter-leaflet P-P distance, ξ, which is used as an order parameter to track leaflet interdigitation (Equation 1). **(c)** Time trace (red) and biphasic linear fits (black) of ξ in cooling simulations of atomistic DPPC membranes. **(d)** Voronoi diagram from the x-y coordinates of the upper leaflet P atoms depicting the area per head group of individual lipids is superimposed on the thickness modulations of membranes at time points I-IV, corresponding to the MD snapshots in (a) (viewing angle pictorially depicted).

Voronoi-thickness membrane maps, which are Voronoi diagrams of the upper membrane leaflet superimposed onto P-P thickness heatmaps[25,43], are shown in Figure 1*d*, corresponding to the top views of MD snapshots in Figure 1*a*. The trends were similar[43] when the Voronoi diagrams were plotted using the lower leaflets (not shown). Compared to the uniform topography in the fluid phase, the formation of interdigitated (blue) and gel (yellow) domains in the ripple phase can be clearly observed. There is negligible difference in membrane topographies between

285 time points III and IV except for the lateral movement of membrane across period boundaries,
286 indicating that the ripple phase membrane configuration at the end of simulated cooling is at
287 equilibrium. An interesting observation was that the interdigitated ripple domain (Figure 1*d*)
288 appeared to be tilted in the lateral plane, whereas ripple domains in previous studies[19,20,43] were
289 typically parallel to one of the lateral box edges. Previous mesoscopic lipid bilayer simulations[21]
290 have revealed that at the highest value of the lipid head-head repulsion parameter explored, lower
291 and higher values of which either abrogated or stabilized the ripple phase, respectively, the bilayer
292 formed a laterally tilted ripple domain and a stable $P_{\beta'}$ membrane phase similar to our
293 observations.

294 Another independent all-atom MD replicate also yielded a similar interdigitated DPPC
295 ripple phase membrane upon cooling (Figure S1*b*), thus validating the robustness of the above
296 MD protocol to produce the $P_{\beta'}$ phase from fluid membrane configurations. We next employed
297 this MD cooling protocol to fluid-phase MARTINI membranes and evaluated their ability to capture
298 the ripple phase.

299

300 **Ripple formation in smaller MARTINI membranes**

301 Fluid phase, 380-lipid, DPPC MARTINI membranes belonging to six MARTINI FF variants
302 were cooled from 350 K to 280 K, and evaluated for their ability to form the interdigitated $P_{\beta'}$
303 membrane phase (see Introduction and Methods). The lower bound for temperature was set to
304 280 K, compared to 290 K for all-atom, because a previous CGMD study showed that ripple-like
305 interdigitated phases in MARTINI DPPC membranes were formed between 280-290 K[36]. The
306 trajectory of an SAMD+EQMD replicate with the MARTINI2n FF is shown with time points I-IV
307 highlighted (Figure 2*a*-*c*). The constant temperature EQMD phase post cooling was chosen to be
308 5 μs for MARTINI (Figure 2*b*), compared to 200 ns for the all-atom simulations (Figure 1*c*). Similar
309 to the time course seen in atomistic DPPC membranes, a majority (70%), but notably not all,

310 MARTINI2n replicates showed interdigitation of membrane leaflets (time points I-IV on the $\xi(t)$
311 plot, Voronoi-thickness maps pertaining to MD snapshots at time points I and IV), thus apparently
312 capturing ripple-like membrane states. This is in accord with previous single replicate studies,
313 where MARTINI membranes of similar sizes captured the ripple phase[31,36,48,49]. In the rest of the
314 MARTINI2n replicates (30%), the membranes bypassed the interdigitated ripple-like state and
315 directly froze into L_β configurations (Figure S2). This emphasizes that with simulated cooling MD,
316 rippling in MARTINI membranes depended on the initial configuration and starting velocities, and
317 therefore necessitated multiple MD replicates for obtaining robust trends.[52]

318 MARTINI SAMD simulations showed two differences compared to all-atom SAMD
319 simulations. Firstly, during SAMD, the atomistic DPPC membranes stay in the fluid phase with
320 disordered tails before the onset of interdigitation (Time point II in Figure 1*a*) and therefore $m_1 \approx$
321 0 (Figure 1*c*; Equation 1). In contrast, $m_1 > 0$ for the MARTINI DPPC membranes since they
322 exhibit a degree of tail ordering and expansion along the Z-axis (compensated by reduced X-Y
323 dimensions) with decreasing temperature before the start of interdigitation (Time point II in Figure
324 2*a*), compared to the fluid phase at 350 K (Time point I in Figure 2*a*). Secondly, the orientation of
325 the interdigitated domains in the MARTINI2n membranes were perpendicular to the x-axis (Figure
326 2*c*), in contrast with the laterally tilted interdigitated domains seen in all-atom simulations (Figures
327 1*d* and S1*b*). Similar domains were observed in a previous MARTINI study.[36]

328 Formation of ripple-like phases in DPPC membranes described by the other FF variants –
329 MARTINI2On, MARTINI3a, MARTINI3b, MARTINI2p, and MARTINI2Op – are summarized in
330 Figures 2*d-g* and S5*b* (all MD replicates for each FF variant displayed in Figures S3-S7).
331 MARTINI2On is similar to MARTINI2n, with 70% of the replicates forming ripple-like (Figures 2*d*
332 and S3). MARTINI3a, the improved[33,51] next generation MARTINI3 FF, showed ripple-like
333 formation in 70% of the replicates, similar to MARTINI2n and MARTINI2On (Figures 2*e* and S4).
334 (The beta version of MARTINI 3 – MARTINI3b – showed ripple-like formation in 20% of the
335 replicates (Figure S5).) The MARTINI FF combinations with polarizable water, MARTINI2p

(Figures 2*f* and S6) and MARTINI2Op (Figures 2*g* and S7), showed ripple-like states in only 10% and 30% of replicates, respectively, despite the reparameterization of polarizable water to improve the accuracy of solvent electrostatic effects[50], important for capturing macroscopic membrane properties[57,58]. Our observations with MARTINI2p are to be contrasted with previous single-replicate MARTINI[36] simulations, where quasi-static cooling of fluid-phase membranes resulted in the formation of the ripple-like domains only with polarizable water. While differences in MD protocols and differences in the initial configurations may explain the disparities, careful future investigations, with systems of varying size, may be necessary to determine the predictive accuracy of polarizable water-lipid interactions.

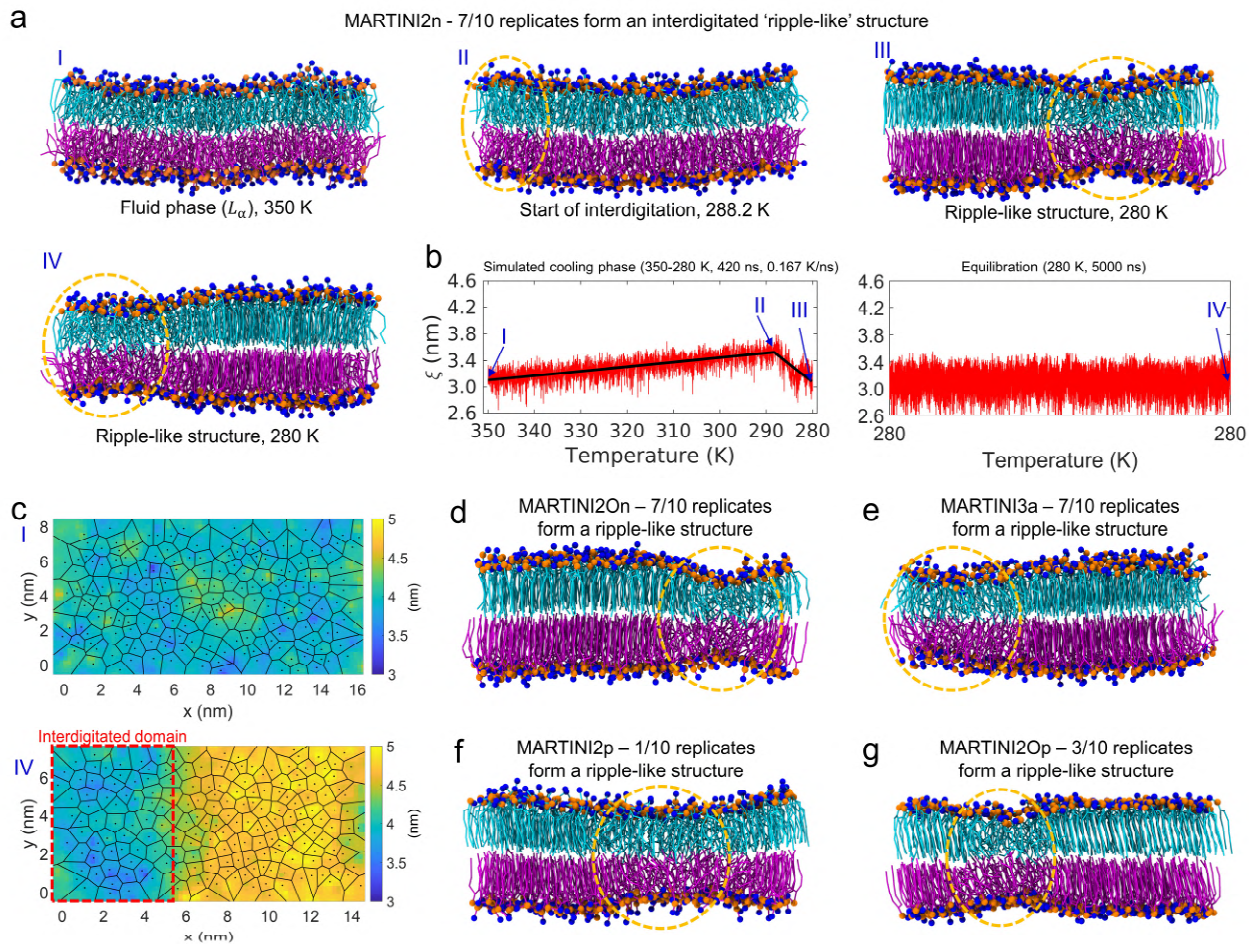

Figure 2. Smaller MARTINI membranes form a ripple-like interdigitated phase upon cooling. (a) Similar to all-atom MD (Figure 1), snapshots from time points I-IV from the simulated

349 cooling of a MARTINI2n membrane replicate from 350 K – 280 K are shown (Replicate 1 from
350 Figure S2). Interdigitated regions are highlighted by a yellow dashed circle. **(b)** Minimum inter-
351 leaflet P-P distance with time in the 420 ns cooling and 5000 ns constant temperature equilibration
352 phases. **(c)** Voronoi-thickness maps contrasting the initial fluid membrane and the final
353 interdigitated ripple-like membrane (time points I and IV, respectively). Cooling of 7/10
354 independent MARTINI2n MD replicates resulted in the formation of a ripple-like phase (Figure
355 S2). Other MARTINI FF variants: **(d)** MARTINI2On (Replicate 5 from Figure S3), **(e)** MARTINI3a
356 (Replicate 5 from Figure S4; MARTINI3b in Figure S5), **(f)** MARTINI2p (Replicate 5 from Figure
357 S6; formed a ripple-like state during EQMD and not SAMD) and **(g)** MARTINI2Op (Replicate 10
358 from Figure S7), show the formation of ripple-like phases in 7, 7, 1 and 3 out of 10 replicates
359 each, respectively. These snapshots correspond to time point IV.

360

361

362 **Testing for ripple formation in large atomistic and MARTINI DPPC membranes upon**
363 **simulated cooling**

364 In a previous study, Rodgers *et al.*[36] observed the interdigitation of lipids in relatively small
365 512-lipid MARTINI DPPC membranes upon quasi-equilibrium, stepwise, simulated cooling of fluid
366 membranes from 325 K to less than 280 K. These small membranes apparently sampled an
367 interdigitated ripple-like phase, similar to our observations (Figure 2). However, when the exercise
368 was repeated with 4-times-larger (2048-lipid) DPPC membranes, the ripple-like phase could not
369 be reproduced. Thus, Rodgers *et al.*[36] concluded that the interdigitated ripple-like states in smaller
370 membranes were actually 'intermediate' kinetically trapped membrane states rather than a true
371 ripple phase. In contrast to these MARTINI simulations, a large all-atom 3200-lipid DPPC
372 membrane has been shown to form an interdigitated ripple phase[31], albeit with a different MD
373 protocol. Therefore, we next tested ripple formation in large all-atom DPPC membranes with our
374 simulated cooling MD protocol (similar to Figure 1), that would re-establish a benchmark to test
375 for ripple formation and system size effects in large MARTINI membranes.

376 We set up two 2208-lipid DPPC bilayer configurations, which were 6-times-larger than the
377 smaller atomistic DPPC membranes shown in Figure 1, and larger than the membranes employed
378 by Rodgers *et al.*[36], and pre-equilibrated them in the L_α phase at 350 K (Figure 3*a*). Subsequently,
379 these membranes were cooled to 290 K with the same SAMD protocol. One of the all-atom MD

380 replicates in the fluid phase formed an interdigitated ripple phase membrane by 290 K (Figure
381 3*b*). The other replicate (Figure S8) formed a non-interdigitated 'symmetric' ripple[20] in the larger
382 dimension, which is typically observed upon slow cooling from the fluid phase to approximately
383 the gel-to-fluid transition temperature[20], and an asymmetric interdigitated ripple (similar to Figures
384 1, 3) in the smaller dimension. Therefore, both smaller and larger all-atom DPPC membranes,
385 described by the CHARMM36 FF, sample the thermodynamic ripple phase upon simulated
386 cooling MD without any evidence of finite size artefacts. In contrast to smaller membranes
387 (Figures 1*d*, S9a, and S1), the Voronoi-thickness map of the first large membrane replicate shows
388 reticulated ripple domains (Figures 3*b* and S9*b*). Our observations are in accord with previous
389 studies[31,45], where simulated quenching of 1280-lipid and 3200-lipid all-atom DPPC membranes
390 to below the main transition temperature also resulted in reticulated ripple domains. Significantly
391 longer runs are probably required to anneal and reorganize these reticulated ripple domains into
392 classically observed periodic ripple domains.

393 We next tested whether large, fluid, rectangular, 2204-lipid MARTINI DPPC membranes,
394 with normal (not polarizable) MARTINI water, also sampled the interdigitated ripple-like phase
395 upon cooling from 350 K to 280 K. Two initial configurations each for MARTINI2n, MARTINI2On,
396 MARTINI3a, and MARTINI3b FFs were set up analogous to the large all-atom membranes in
397 Figure 3, and pre-equilibrated at 350 K, followed by cooling to 280 K (Figures 4 and S10).
398 However, none of the large MARTINI membranes captured a ripple-like phase upon cooling to
399 280 K. MARTINI2n and MARTINI3a/b membranes directly froze into the L_β phase, while the
400 MARTINI2On membranes transitioned to the $L_{\beta'}$ phase (Figure 4b); confirmed by independent
401 MD replicates (Figure S10). To ensure that membrane geometry did not influence these results,
402 we repeated these simulations with large 6728-lipid square MARTINI2On membranes, and these
403 also did not sample ripple-like states (Figure S11). Since only smaller (380-lipid) but not larger
404 (>2204-lipid) DPPC MARTINI membranes captured the interdigitated ripple-like states, in contrast
405 to all-atom membranes, we inferred that the smaller MARTINI ripple-like membranes (Figures 2,

S2-S7) represent kinetically-trapped states caused by finite box-size effects rather than true ripple states.

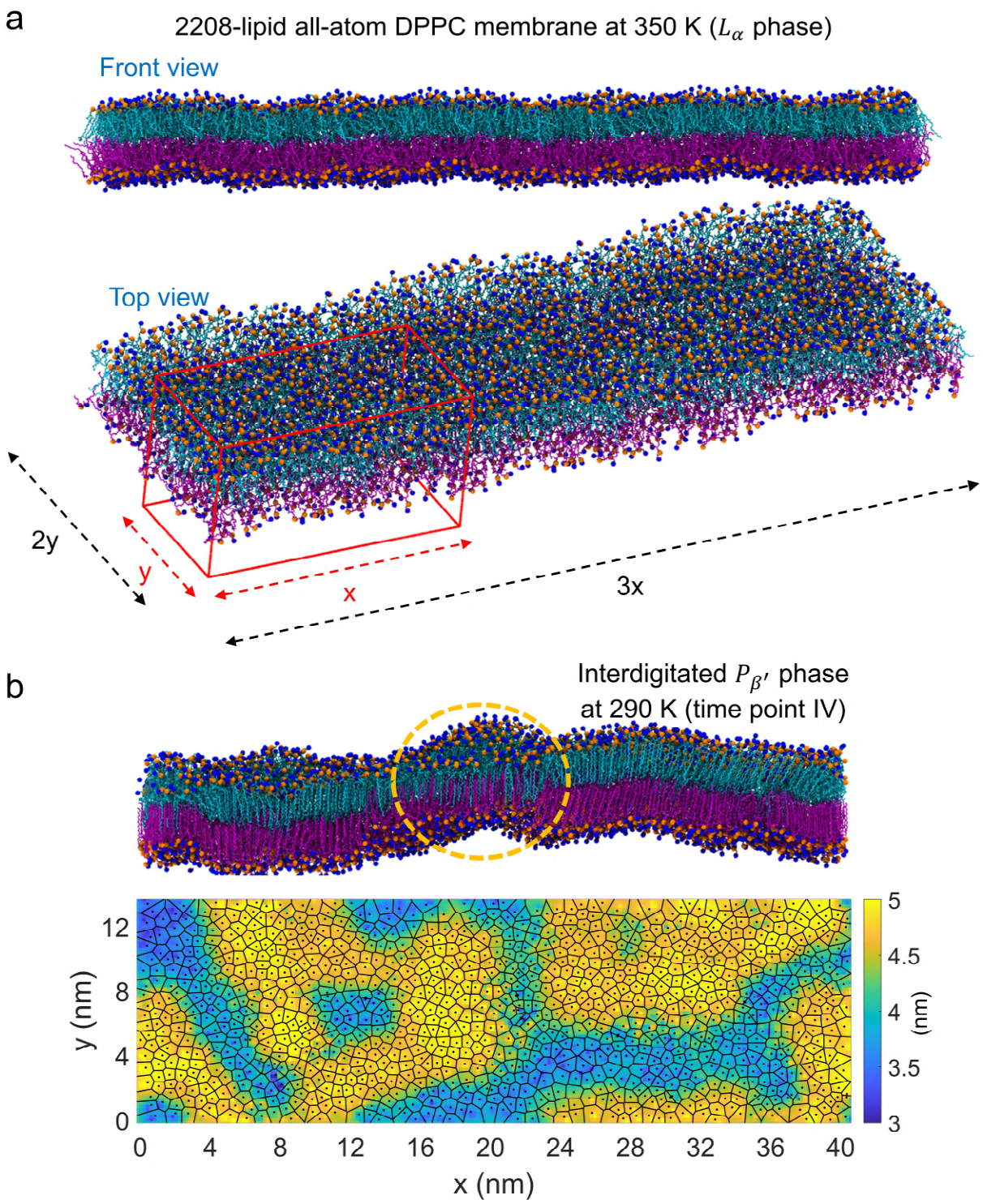

410 **Figure 3. Ripple formation from all-atom MD of a large DPPC membrane. (a)** Front and top
411 views of a large 2208-lipid DPPC membrane which was pre-equilibrated in the fluid phase at 350
412 K. For comparison, a representative simulation box of a smaller all-atom membrane (Figure 1) is
413 shown in red. The large membrane is 6-times (3X times 2Y) larger than the smaller membrane.
414 **(b)** Front view of the large membrane after cooling to 290 K and EQMD (corresponds to time point
415 IV), and its Voronoi-thickness modulation map (blue represents interdigitated regions) shows the
416 formation of an aperiodic and reticulated interdigitated ripple domain (also see Figures S8-S9).

417

418 **Equilibrium MD simulations of large MARTINI membranes initialized in the ripple-like**
419 **phase show loss of interdigitation**

420 To confirm the aforementioned inference, we employed an orthogonal approach where
421 multi-μs equilibrium simulations of large MARTINI membranes, initialized in periodic interdigitated
422 ripple-like configurations, were performed at 280 K. These large systems were created from the
423 final, interdigitated, ripple-like, smaller (380-lipid) MARTINI membrane configurations after 1 μs
424 of constant temperature EQMD at 280 K. The smaller membranes were repeated 6-times along
425 the lateral bilayer plane across periodic boundaries (3x times 2y), and the initial large 2280-lipid
426 ripple-like membrane configurations thus created are displayed in Figures 5*a, c, d* and S12*d*,
427 corresponding to MARTINI2On, MARTINI2n, MARTINI3a, and MARTINI3b, respectively.

428 The rationale behind performing equilibrium MD of these large systems was simply to test
429 if the ripple-like states in small systems were stabilized due to finite size effects. Upon 3-10 μs of
430 constant temperature NPT-MD at 280 K, we observed that the large, interdigitated MARTINI
431 membranes spontaneously froze into the gel phase, as shown by both MD snapshots (Figures 5
432 and S12*d*) and Voronoi-thickness maps (Figure S12*a-d*), indicating that the initial ripple-like
433 membrane configuration was unfavourable at larger system sizes. This phenomenon was
434 observed for all the four MARTINI FF variants, although the time scale over which interdigitation
435 disappeared leading to formation of the final gel phase configuration varied amongst the FFs.
436 MARTINI2On showed progressive loss of interdigitation which was nearly complete by 8 μs
437 (Figures 5*b* and S10*a*). Longer simulations may have shown a complete loss of interdigitation,
438 but we did not further pursue these computationally intensive MD simulations since the

439 progressive loss of interdigitation with time was apparent (Figures 5*a, b* and S12*a*). MARTINI2n
440 showed a rapid and complete loss of interdigitation by 3 μs (Figures 5*c* and S12*b*), and
441 MARTINI3a/b showed near-complete loss of interdigitation by 10 μs (Figures 5*d* and S12*c, d*),
442 similar to MARTINI2On. In contrast, none of the smaller membranes showed any loss of
443 interdigitation upon 5 μs of constant temperature EQMD at 280 K (Figures 2 and S5*b*).

444 Together with observations from the simulated cooling of large fluid membranes, these two
445 orthogonal MD approaches (Figures 4, 5, S10-12) strongly suggest that MARTINI membranes
446 (with all the tested FFs) do not capture the thermodynamic ripple phase, unlike all-atom
447 membranes. Our systematic study implies that ripple-like phase formation observed in smaller
448 MARTINI membranes was due to kinetic trapping of interdigitated leaflets at small system sizes.
449 The few studies which indeed report MARTINI ripple phase membranes, both with[49] and
450 without[36,48] enhanced sampling, are with smaller membranes composed of 390[49] and 512[36,48]
451 lipids, respectively. Therefore, based on our observations, the formation of rippled bilayers in
452 these studies could be attributed to finite size artefacts[36] until they are validated with simulations
453 at larger system sizes. Thus, MARTINI FF parameters may have to be tuned to better reproduce
454 the lipid membrane phase diagram, and the $P_{\beta'}$ phase in particular. FF approaches that tune the
455 bonded parameters of MARTINI lipids based on comparison with all-atom simulations[25,31,36] may
456 result in models that better capture membrane phase behaviour.

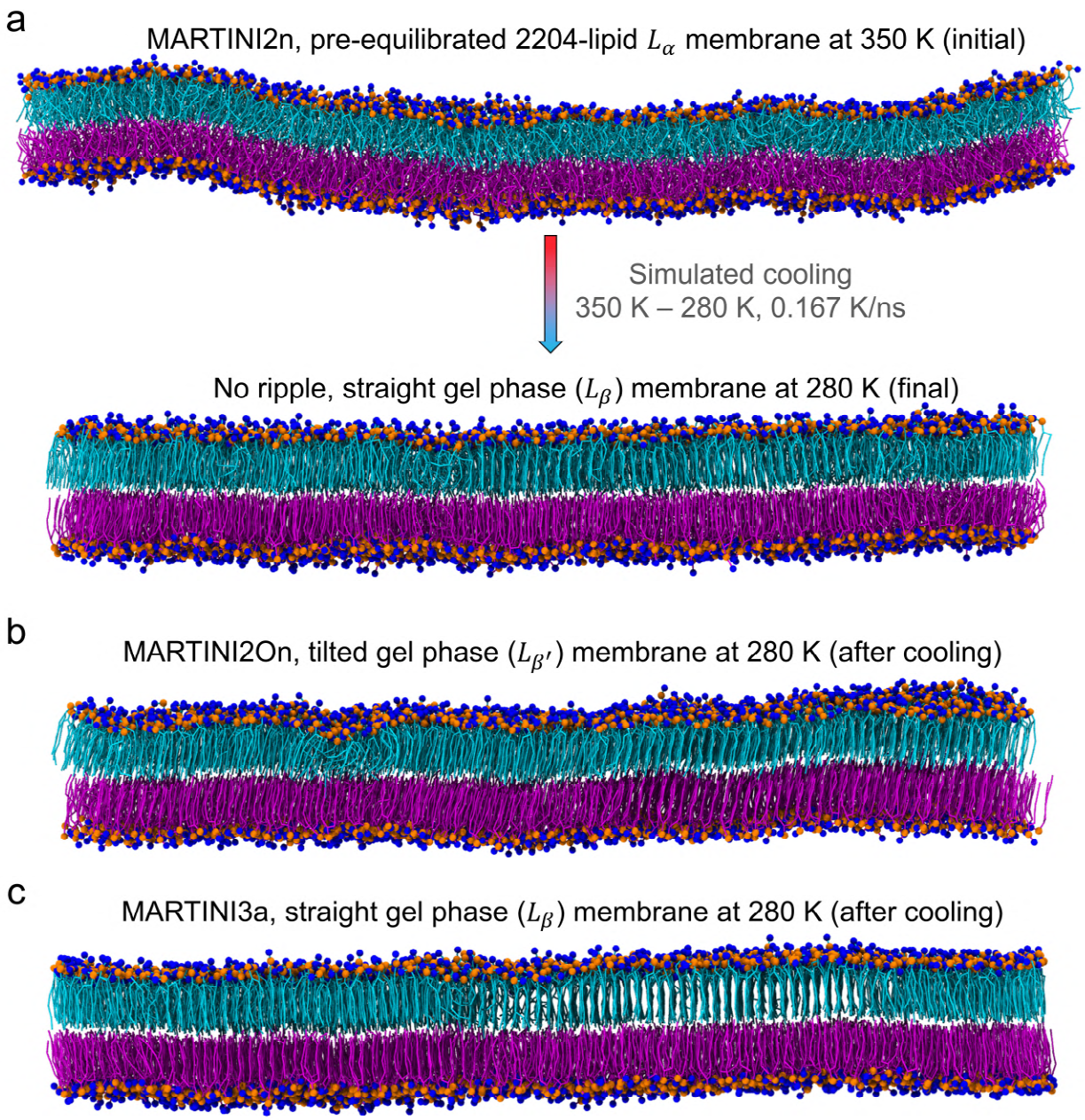

Figure 4. Lack of ripple formation in large MARTINI DPPC membranes. (a) A representative 2204-lipid, rectangular, MARTINI2n DPPC membrane, pre-equilibrated at 350 K in the L_α phase, was cooled directly into the gel phase at 280 K without the membrane sampling a ripple-like phase, unlike all-atom systems (see Figure 3). This behaviour was also observed with **(b)** MARTINI2On and **(c)** MARTINI3a FFs. Independent MD replicates are shown in Figure S10. Two independent simulation replicates, where large 6728-lipid, square, MARTINI2On membranes were cooled to 290 K, also showed a similar lack of sampling of a ripple-like phase (Figure S11), suggesting that system geometry did not influence our observations.

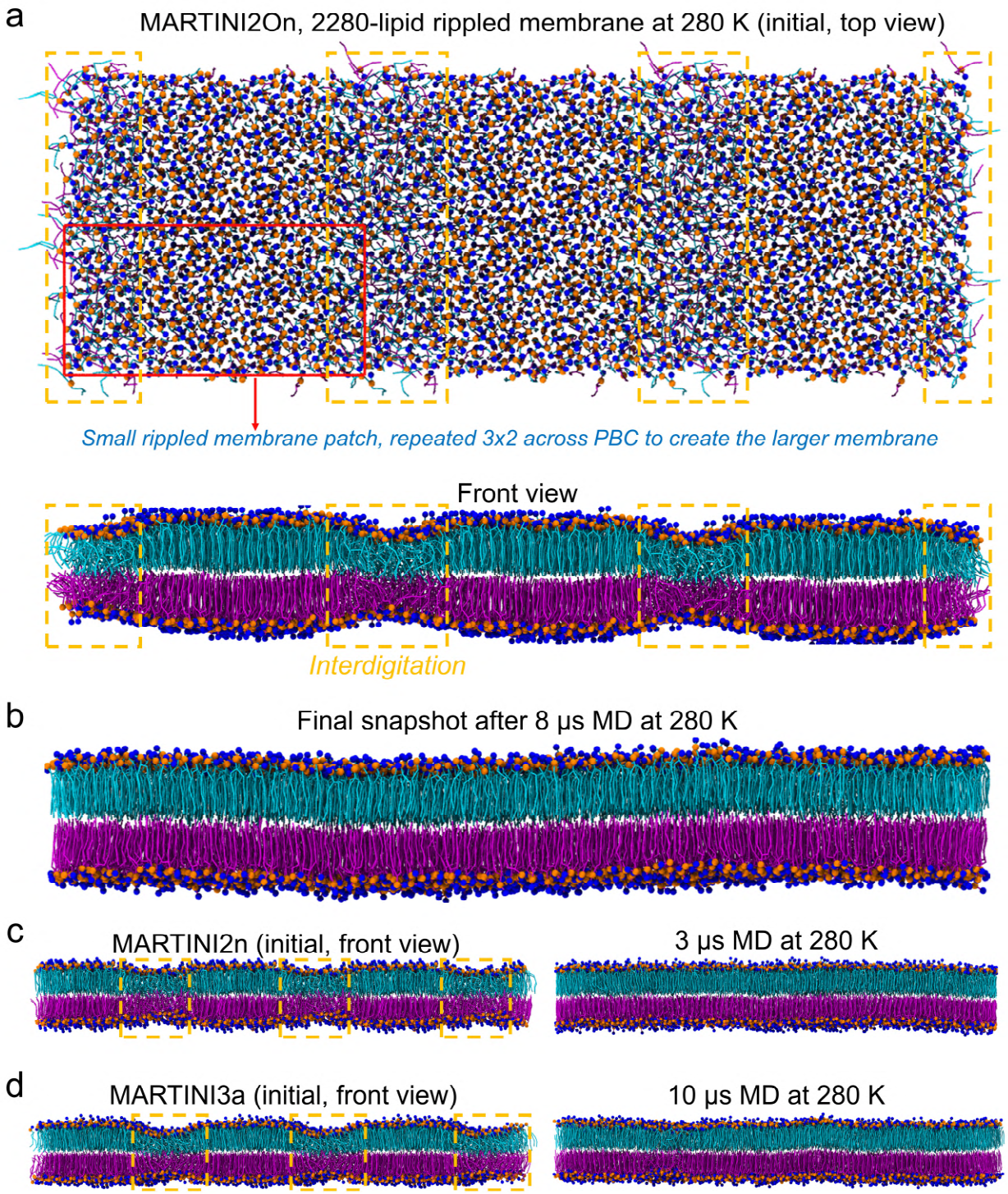

Figure 5. MD simulations of large MARTINI DPPC membranes starting with interdigitated ripple-like states. (a) To test the stability of kinetically trapped domains (yellow dashed rectangles) at larger system sizes, a 2280-lipid MARTINI2On DPPC membrane configuration with periodic ripples (top and front views) was created by repeating smaller ripple-like membranes (from time point IV, Figure 2d) six-times across periodic boundary conditions (thrice in X, twice in Y). **(b)** 8 μs MD at 280 K almost completely abolished the interdigitated ripple-like configuration and led to the establishment of the L_β phase (Voronoi-thickness maps in Figure S12*a*). Similar

476 loss of the ripple-like domains was seen for large MARTINI2n **(c),** and MARTINI3a **(d),**
477 membranes (Voronoi-thickness maps in Figure S12*b, c*).

478

479 **The optimized MARTINI DPPC FF (MARTINI2On) forms the $L_{\beta'}$, but not $P_{\beta'}$, phase**

480 DPPC, with its large headgroup and strong head-head interactions, favours a tilted gel
481 ($L_{\beta'}$) phase at lower temperatures. Therefore, during the L_{α} → $L_{\beta'}$ transition upon simulated
482 cooling, the tilted ripple ($P_{\beta'}$) state occurs. Lipids exhibiting an L_{β} state at lower temperatures,
483 such as phosphatidylethanolamines[75], show a single phase transition and do not form the ripple
484 phase[20]. In our small membrane simulations, MARTINI2n (Figure S2) and MARTINI3a/b (Figures
485 S4 and S5) mostly froze into L_{β} states below transition temperatures, in accord with previous
486 studies[36,49]. MARTINI2n was previously shown to sample the $L_{\beta'}$ phase only upon enhanced
487 sampling[76]. The frozen lipids in the upper leaflet of replicate 2 of MARTINI3a (Figure S4) are
488 weakly tilted, suggesting that this FF may also capture the $L_{\beta'}$ phase upon enhanced sampling.
489 This propensity to freeze into the L_{β} state may underlie the inability of these FFs to capture the
490 $P_{\beta'}$ phase. However, MARTINI2On, possessing optimized DPPC bond parameters that closely
491 match macroscopic membrane properties from all-atom simulations, spontaneously captured the
492 $L_{\beta'}$ phase in many of the small membrane replicates upon cooling with classical MD simulations
493 (Figure S3). This agrees with a previous study[31] that developed the MARTINI2On DPPC
494 parameters, where the authors also observed the formation of the $L_{\beta'}$ phase without enhanced
495 sampling. Even in replicates that formed interdigitated ripple-like configurations (Figure S3), the
496 non-interdigitated gel-like domains often resembled the $L_{\beta'}$ phase.

497 To further contrast the lipid tilt in the gel phase configurations of DPPC MARTINI2n and
498 MARTINI2On membranes, we chose representative replicates (#7 in Figure S2, #3 and #7 in
499 Figure S3) that had frozen into gel states after SAMD without sampling interdigitated ripple-like
500 states, and further equilibrated them at 280 K for 5 μs in the NPT ensemble. The final MD

501 snapshots for MARTINI2n (#7 from Figure S2) and MARTINI2On (#7 from Figure S3) are
502 illustrated in Figure 6*a, b*. Clearly, MARTINI2n and MARTINI2On form stable L_β and $L_{\beta'}$
503 configurations, respectively, at 280 K. For both systems, we quantified the extent of lipid tilt from
504 the tilt angle (θ°) distributions of lipids with their respective leaflet normal (Methods; Figure 6*c*).
505 The MARTINI2n and MARTINI2On gel phase tilt distributions were observed to have modes at
506 7.3° and 15.2°, respectively.

507 To ensure that the MARTINI2On $L_{\beta'}$ configuration was not a consequence of finite size
508 artefacts, we created a 6-times-larger membrane by repeating the membrane from Figure 6*b*
509 across periodic boundaries (3x times 2y; similar to Figure 5). This initial configuration is shown in
510 Figure 6*d*, and was simulated at 280 K for 5 μs. From the final snapshot (Figure 6*d*), the $L_{\beta'}$
511 configuration is completely preserved. Additionally, simulated cooling of a large L_α MARTINI2On
512 membrane from 350 K – 280 K also resulted in a $L_{\beta'}$ configuration (Figure 4*b*). These observations
513 strongly suggest that MARTINI2On membranes can sample the true $L_{\beta'}$ phase at lower
514 temperatures, without any finite size artefacts, and in agreement with previous studies[31].
515 However, our multi-replicate simulations show that MARTINI2On membranes also stochastically
516 sample the L_β phase, as shown by replicates #2 and #8 in smaller membranes (Figure S3), and
517 from the simulations of large membranes (Figures 5*b*, S10 and S11). Therefore, there may be
518 room for further optimization of the MARTINI2On DPPC FF for accurate reproduction of low
519 temperature phase behaviour.

520 Interestingly, when replicate #3 from Figure S3 was equilibrated for 5 μs at 280 K, it showed
521 the formation of a weakly interdigitated titled domain (Figure S13*a*), a potential precursor for the
522 formation of a true ripple phase. To assess this further, we set up a 6-times larger membrane
523 (Figure S13*b*) by repeating the smaller system across periodic boundaries along the membrane
524 plane (similar to Figure 5*a*). After 10 μs of constant temperature EQMD at 280 K, the interdigitation

almost completely disappeared as shown by the final MD snapshot (Figure S13*b*) and corresponding Voronoi-thickness maps (Figure S13*c*).

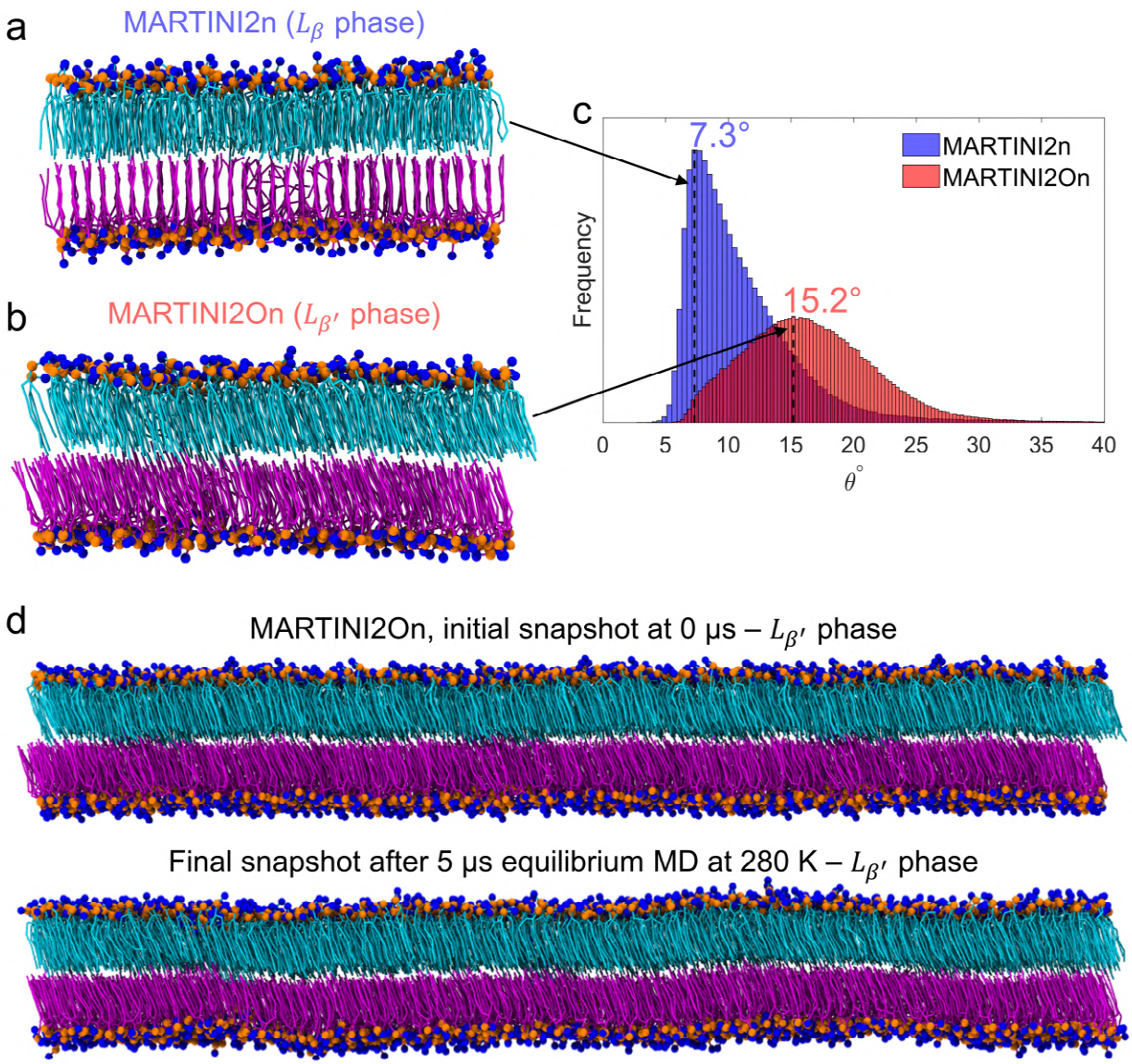

Figure 6. Comparison of gel-phase structures of MARTINI membranes. Gel phase DPPC bilayer structures with **(a)** the standard MARTINI2n FF, and **(b)** the optimized MARTINI2On FF are shown. MARTINI2n membranes freeze into the straight gel phase (L_β) whereas MARTINI2On membranes often sample the tilted gel phase ($L_{\beta'}$), quantified by the lipid tilt-angle distributions **(c)**. **(d)** To confirm that this was a true thermodynamic phase and not a finite size effect, the smaller $L_{\beta'}$ membrane in (a) was replicated 6x (initial snapshot) and then equilibrated for 5 μs at 280 K. The membrane remained in the $L_{\beta'}$ phase thus ruling out finite size artefacts.

537 ## Conclusions

538 Molecular simulations at various levels of FF descriptions, ranging from all-atom and united
539 atom models at the finer scales to DPD and MARTINI models at higher levels of coarse graining,
540 have been extensively used to study the rich variety of equilibrium phases observed in model
541 phospholipid bilayer membranes[1,17,77]. In particular, the rippled $P_{\beta'}$ phase, sensitive to initial
542 configurations, annealing protocols, and finite-size effects, has been challenging to capture using
543 MD simulations[20,25,36,43]. Although all-atom FFs have successfully captured the formation of the
544 ripple phase (Table 1), the ability of the widely used MARTINI force-fields to stabilize this
545 intermediate phase, which occurs below the main gel-to-liquid crystalline transition, has been a
546 matter of some debate[36,49].

547 In this manuscript, we assessed the ability of MARTINI DPPC lipid membranes described
548 by six MARTINI FF variants (see Introduction and Methods) towards capturing the ripple phase.
549 Previous experiments[35,39–42] and all-atom simulations[19,31,45,46] have shown that DPPC
550 membranes sample the tilted ripple phase at pre-transition temperatures. Previous MARTINI
551 studies yielded conflicting observations, with some inferring that MARTINI DPPC lipid membranes
552 could not capture the ripple state[36], while other studies observed otherwise[31,48,49]. Therefore, we
553 established a standard simulated annealing-based MD protocol, built on insights from previous
554 studies[18–20,31,45,46], for reliably producing the tilted ripple phase in multiple all-atom DPPC
555 membrane MD replicates. By cooling from the fluid phase to below the phase transition followed
556 by constant temperature equilibration. The structure of these rippled membranes resembled those
557 from previous studies[19,20,45,46]. We then applied the same MD protocol to fluid phase MARTINI
558 DPPC membranes with six MARTINI FF variants and ten independent MD replicates per variant.
559 Simulations with all the MARTINI FFs showed that a fraction of replicates formed interdigitated
560 ripple-like states. These simulations also reinforced the importance of using multiple independent
561 MD replicates for robustly observing phase behaviour[18,52]. The lateral orientation of interdigitated

562 domains in these ripple-like membranes were different compared to those from all-atom
563 simulations and resembled a membrane with co-existing interdigitated L_α and gel phases.

564 Next, we explored whether the MARTINI ripple-like membranes were kinetically trapped
565 states enforced by finite system size effects. To this end, we first re-established the all-atom
566 protocols by employing the aforementioned MD cooling protocol on large all-atom DPPC
567 membranes. We observed that these larger membranes also formed the tilted ripple phase with
568 reticulated interdigitated domains, in agreement with previously reported large-membrane all-
569 atom DPPC simulations[31,45]. However, when similarly large MARTINI DPPC membranes (4 FF
570 variants, 2 replicates each) were cooled from the fluid phase, they failed to capture ripple-like
571 states and froze directly into the gel phase . To confirm this behaviour via an orthogonal approach,
572 we created larger membranes from previously formed smaller ripple-like membranes, by
573 repeating them across periodic boundaries. These larger MARTINI periodic ripple-like
574 membranes (4 FF variants), with an initial configuration bias towards the ripple phase, were then
575 simulated at a constant temperature of 280 K, below the transition temperature. Strikingly, all the
576 membranes showed a progressive loss of the interdigitated ripple-like domains, and either
577 transitioned, or were in the process of transitioning, into the gel phase. Based on these findings
578 we attribute the ripple-like states observed in the smaller MARTINI membranes to finite size
579 artefacts. In the case of the MARTINI2On DPPC FF, the inability to form the tilted ripple was
580 despite its ability to capture the tilted gel phase at lower temperatures without the need for
581 enhanced sampling.

582 In summary, our systematic observations suggest that the current MARTINI DPPC FFs,
583 including the recently developed MARTINI3, may not be able to capture the $P_{\beta'}$ phase, which
584 involves an intricate interplay of lipid tail interdigitation, tilt and headgroup hydration in the ripple
585 state of the membrane. CG force fields like MARTINI are known to overestimate enthalpy to
586 compensate for an intrinsically low entropy due to reduced degrees of freedom[78]. Specifically
587 reparametrizing the MARTINI FFs to correct this enthalpy-entropy imbalance and better

reproduce membrane thermodynamics as well as phase behaviour is expected to yield improved CG models that may bridge the qualitative and quantitative gap towards all-atom MD simulations, while unlocking the speed and scaling advantages associated with the versatile and powerful MARTINI framework.

Acknowledgements

We thank the Supercomputer Education and Research Center (SERC) computational facility at the Indian Institute of Science, Bengaluru, for access to supercomputing resources. K.G.A. acknowledges funding by a grant from the Department of Science and Technology, Government of India.

Conflict of interest

The authors declare no conflicts of interest.

Supporting information

Supporting information contains detailed author contributions, and thirteen supporting figures, namely: an all-atom MD simulation replicate reproducing the ripple phase (Figure S1), ten independent cooling MD simulation replicates with the six MARTINI FFs (Figures S2-S7), and large all-atom (Figures S8 and S9) and MARTINI (Figures S10-S13) membrane simulations.

TOC Graphic

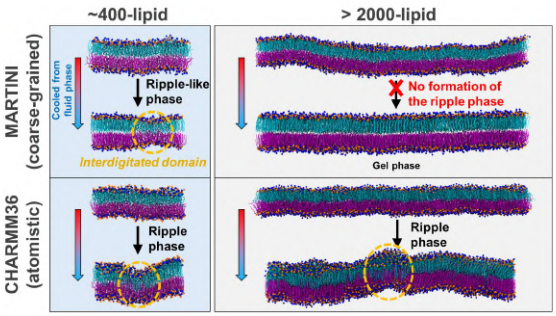

References

(1) Kulkarni, C. V. Lipid Crystallization: From Self-Assembly to Hierarchical and Biological Ordering. *Nanoscale* **2012**, *4* (19), 5779–5791.

(2) Nagle, J. F. Theory of the Main Lipid Bilayer Phase Transition. *Ann. Rev. Phys. Chem.* **1980**, *31* (1), 157–196.

(3) Harayama, T.; Riezman, H. Understanding the Diversity of Membrane Lipid Composition. *Nat. Rev. Mol. Cell Biol.* **2018**, *19* (5), 281–296.

(4) Kohli, A. G.; Kierstead, P. H.; Venditto, V. J.; Walsh, C. L.; Szoka, F. C. Designer Lipids for Drug Delivery: From Heads to Tails. *J. Control. Release* **2014**, *190*, 274–287.

(5) Anderson, M.; Omri, A. The Effect of Different Lipid Components on the in Vitro Stability and Release Kinetics of Liposome Formulations. *Drug. Deliv.* **2004**, *11* (1), 33–39.

(6) Kulkarni, A.; Chandrasekar, V.; Natarajan, S. K.; Ramesh, A.; Pandey, P.; Nirgud, J.; Bhatnagar, H.; Ashok, D.; Ajay, A. K.; Sengupta, S. A Designer Self-Assembled Supramolecule Amplifies Macrophage Immune Responses against Aggressive Cancer. *Nat. Biomed. Eng.* **2018**, *2* (8), 589–599.

(7) Phillips, R.; Ursell, T.; Wiggins, P.; Sens, P. Emerging Roles for Lipids in Shaping Membrane-Protein Function. *Nature* **2009**, *459* (7245), 379–385.

(8) Blicher, A.; Wodzinska, K.; Fidorra, M.; Winterhalter, M.; Heimburg, T. The Temperature Dependence of Lipid Membrane Permeability, Its Quantized Nature, and the Influence of Anesthetics. *Biophys. J.* **2009**, *96* (11), 4581–4591.

(9) Sharma, P.; Parthasarathi, S.; Patil, N.; Waskar, M.; Raut, J. S.; Puranik, M.; Ayappa, K. G.; Basu, J. K. Assessing Barriers for Antimicrobial Penetration in Complex Asymmetric Bacterial Membranes: A Case Study with Thymol. *Langmuir* **2020**, *36* (30), 8800–8814.

(10) Perez-Isidoro, R.; Sierra-Valdez, F. J.; Ruiz-Suarez, J. C. Anesthetic Diffusion through Lipid Membranes Depends on the Protonation Rate. *Sci. Rep.* **2014**, *4*, 7534.

(11) Yilmaz, N.; Kobayashi, T. Assemblies of Pore-Forming Toxins Visualized by Atomic Force Microscopy. *Biochim. Biophys. Acta* **2016**, *1858* (3), 500–511.

(12) Rojko, N.; Anderluh, G. How Lipid Membranes Affect Pore Forming Toxin Activity. *Acc. Chem. Res.* **2015**, *48* (12), 3073–3079.

(13) Gerelli, Y.; Porcar, L.; Lombardi, L.; Fragneto, G. Lipid Exchange and Flip-Flop in Solid Supported Bilayers. *Langmuir* **2013**, *29* (41), 12762–12769.

(14) Pomorski, T. G.; Menon, A. K. Lipid Somersaults: Uncovering the Mechanisms of Protein-Mediated Lipid Flipping. *Prog. Lipid Res.* **2016**, *64*, 69–84.

(15) Andersen, S. S.; Jackson, A. D.; Heimburg, T. Towards a Thermodynamic Theory of Nerve Pulse Propagation. *Prog. Neurobiol.* **2009**, *88* (2), 104–113.

(16) de Smet, M.; Langereis, S.; van den Bosch, S.; Grull, H. Temperature-Sensitive Liposomes for Doxorubicin Delivery under MRI Guidance. *J. Control. Release* **2010**, *143* (1), 120–127.

(17) Enkavi, G.; Javanainen, M.; Kulig, W.; Róg, T.; Vattulainen, I. Multiscale Simulations of Biological Membranes: The Challenge To Understand Biological Phenomena in a Living Substance. *Chem. Rev.* **2019**, *119* (9), 5607–5774.
(18) Sun, L.; Böckmann, R. A. Membrane Phase Transition during Heating and Cooling: Molecular Insight into Reversible Melting. *Eur. Biophys. J.* **2018**, *47* (2), 151–164.
(19) Vries, A. H. de; Yefimov, S.; Mark, A. E.; Marrink, S. J. Molecular Structure of the Lecithin Ripple Phase. *PNAS* **2005**, *102* (15), 5392–5396.
(20) Lenz, O.; Schmid, F. Structure of Symmetric and Asymmetric ``Ripple'' Phases in Lipid Bilayers. *Phys. Rev. Lett.* **2007**, *98* (5), 058104.
(21) Kranenburg, M.; Smit, B. Phase Behavior of Model Lipid Bilayers. *J. Phys. Chem. B* **2005**, *109* (14), 6553–6563.
(22) Marrink, S. J.; Tieleman, D. P. Perspective on the Martini Model. *Chem. Soc. Rev.* **2013**, *42* (16), 6801–6822.
(23) Marrink, S. J.; Risselada, H. J.; Yefimov, S.; Tieleman, D. P.; de Vries, A. H. The MARTINI Force Field: Coarse Grained Model for Biomolecular Simulations. *J. Phys. Chem. B* **2007**, *111* (27), 7812–7824.
(24) Bruininks, B. M. H.; Souza, P. C. T.; Marrink, S. J. A Practical View of the Martini Force Field. In *Biomolecular Simulations: Methods and Protocols*; Bonomi, M., Camilloni, C., Eds.; Methods in Molecular Biology; Springer: New York, NY, 2019; pp 105–127.
(25) Srivastava, A.; Debnath, A. Asymmetry and Rippling in Mixed Surfactant Bilayers from All-Atom and Coarse-Grained Simulations: Interdigitation and Per Chain Entropy. *J. Phys. Chem. B* **2020**.
(26) Vaiwala, R.; Sharma, P.; Puranik, M.; Ayappa, K. G. Developing a Coarse-Grained Model for Bacterial Cell Walls: Evaluating Mechanical Properties and Free Energy Barriers. *J. Chem. Theory Comput.* **2020**, *16* (8), 5369–5384.
(27) Ingólfsson, H. I.; Melo, M. N.; van Eerden, F. J.; Arnarez, C.; Lopez, C. A.; Wassenaar, T. A.; Periole, X.; de Vries, A. H.; Tieleman, D. P.; Marrink, S. J. Lipid Organization of the Plasma Membrane. *J. Am. Chem. Soc.* **2014**, *136* (41), 14554–14559.
(28) Alessandri, R.; Souza, P. C. T.; Thallmair, S.; Melo, M. N.; de Vries, A. H.; Marrink, S. J. Pitfalls of the Martini Model. *J. Chem. Theory Comput.* **2019**, *15* (10), 5448–5460.
(29) Desikan, R.; Patra, S. M.; Sarthak, K.; Maiti, P. K.; Ayappa, K. G. Comparison of Coarse-Grained (MARTINI) and Atomistic Molecular Dynamics Simulations of α and β Toxin Nanopores in Lipid Membranes. *J. Chem. Sci.* **2017**, *129* (7), 1017–1030.
(30) Desikan, R.; Behera, A.; Maiti, P. K.; Ayappa, K. G. Chapter Sixteen - Using Multiscale Molecular Dynamics Simulations to Obtain Insights into Pore Forming Toxin Mechanisms. In *Methods in Enzymology*; Heuck, A. P., Ed.; Pore-Forming Toxins; Academic Press, 2021; Vol. 649, pp 461–502.
(31) Carpenter, T. S.; López, C. A.; Neale, C.; Montour, C.; Ingólfsson, H. I.; Di Natale, F.; Lightstone, F. C.; Gnanakaran, S. Capturing Phase Behavior of Ternary Lipid Mixtures with a Refined Martini Coarse-Grained Force Field. *J. Chem. Theory Comput.* **2018**, *14* (11), 6050–6062.
(32) Globisch, C.; Krishnamani, V.; Deserno, M.; Peter, C. Optimization of an Elastic Network Augmented Coarse Grained Model to Study CCMV Capsid Deformation. *PLoS ONE* **2013**, *8* (4), e60582.
(33) Souza, P. C. T.; Alessandri, R.; Barnoud, J.; Thallmair, S.; Faustino, I.; Grünewald, F.; Patmanidis, I.; Abdizadeh, H.; Bruininks, B. M. H.; Wassenaar, T. A. et al. Martini 3: A General Purpose Force Field for Coarse-Grained Molecular Dynamics. *Nat. Methods* **2021**, *18* (4), 382–388.
(34) Biltonen, R. L.; Lichtenberg, D. The Use of Differential Scanning Calorimetry as a Tool to Characterize Liposome Preparations. *Chem. Phys. Lipids* **1993**, *64* (1), 129–142.
(35) Tardieu, A.; Luzzati, V.; Reman, F. C. Structure and Polymorphism of the Hydrocarbon Chains of Lipids: A Study of Lecithin-Water Phases. *J. Mol. Biol.* **1973**, *75* (4), 711–733.

(36) Rodgers, J. M.; Sorensen, J.; de Meyer, F. J.; Schiott, B.; Smit, B. Understanding the Phase Behavior of Coarse-Grained Model Lipid Bilayers through Computational Calorimetry. *J. Phys. Chem. B* **2012**, *116* (5), 1551–1569.
(37) Riske, K. A.; Barroso, R. P.; Vequi-Suplicy, C. C.; Germano, R.; Henriques, V. B.; Lamy, M. T. Lipid Bilayer Pre-Transition as the Beginning of the Melting Process. *Biochim. Biophys. Acta Biomembr.* **2009**, *1788* (5), 954–963.
(38) Heimburg, T. A Model for the Lipid Pretransition: Coupling of Ripple Formation with the Chain-Melting Transition. *Biophys. J.* **2000**, *78* (3), 1154–1165.
(39) Sun, W. J.; Tristram-Nagle, S.; Suter, R. M.; Nagle, J. F. Structure of the Ripple Phase in Lecithin Bilayers. *PNAS* **1996**, *93* (14), 7008–7012.
(40) Katsaras, J.; Tristram-Nagle, S.; Liu, Y.; Headrick, R. L.; Fontes, E.; Mason, P. C.; Nagle, J. F. Clarification of the Ripple Phase of Lecithin Bilayers Using Fully Hydrated, Aligned Samples. *Phys. Rev. E* **2000**, *61* (5), 5668–5677.
(41) Sengupta, K.; Raghunathan, V. A.; Katsaras, J. Structure of the Ripple Phase of Phospholipid Multibilayers. *Phys. Rev. E* **2003**, *68* (3), 031710.
(42) Kamal, M. A.; Raghunathan, V. Naphthalene Derivatives Induce Acyl Chain Interdigitation in Dipalmitoylphosphatidylcholine Bilayers. *J. Phys. Chem. B* **2016**, *120* (1), 164–172.
(43) Debnath, A.; Thakkar, F. M.; Maiti, P. K.; Kumaran, V.; Ayappa, K. G. Laterally Structured Ripple and Square Phases with One and Two Dimensional Thickness Modulations in a Model Bilayer System. *Soft Matter* **2014**, *10* (38), 7630–7637.
(44) Pluhackova, K.; Kirsch, S. A.; Han, J.; Sun, L.; Jiang, Z.; Unruh, T.; Böckmann, R. A. A Critical Comparison of Biomembrane Force Fields: Structure and Dynamics of Model DMPC, POPC, and POPE Bilayers. *J. Phys. Chem. B* **2016**, *120* (16), 3888–3903.
(45) Kirsch, S. A.; Böckmann, R. A. Coupling of Membrane Nanodomain Formation and Enhanced Electroporation near Phase Transition. *Biophys. J.* **2019**, *116* (11), 2131–2148.
(46) Khakbaz, P.; Klauda, J. B. Investigation of Phase Transitions of Saturated Phosphocholine Lipid Bilayers via Molecular Dynamics Simulations. *Biochim. Biophys. Acta Biomembr.* **2018**, *1860* (8), 1489–1501.
(47) Debnath, A.; Ayappa, K. G.; Kumaran, V.; Maiti, P. K. The Influence of Bilayer Composition on the Gel to Liquid Crystalline Transition. *J. Phys. Chem. B* **2009**, *113* (31), 10660–10668.
(48) Lin, X.; Gu, N. Surface Properties of Encapsulating Hydrophobic Nanoparticles Regulate the Main Phase Transition Temperature of Lipid Bilayers: A Simulation Study. *Nano Res.* **2014**, *7* (8), 1195–1204.
(49) Stelter, D.; Keyes, T. Enhanced Sampling of Phase Transitions in Coarse-Grained Lipid Bilayers. *J. Phys. Chem. B* **2017**, *121* (23), 5770–5780.
(50) Yesylevskyy, S. O.; Schäfer, L. V.; Sengupta, D.; Marrink, S. J. Polarizable Water Model for the Coarse-Grained MARTINI Force Field. *PLoS Comput. Biol.* **2010**, *6* (6), 1–17.
(51) Souza, P. C. T. and Marrink, S. J. MARTINI 3 – Open Beta-Release. *The MARTINI web portal* (http://cgmartini.nl), 2020.
(52) Grossfield, A.; Patrone, P. N.; Roe, D. R.; Schultz, A. J.; Siderius, D.; Zuckerman, D. M. Best Practices for Quantification of Uncertainty and Sampling Quality in Molecular Simulations [Article v1.0]. *Living J. Comp. Mol. Sci.* **2018**, *1* (1), 5067.
(53) Jo, S.; Kim, T.; Iyer, V. G.; Im, W. CHARMM-GUI: A Web-Based Graphical User Interface for CHARMM. *J. Comput. Chem.* **2008**, *29* (11), 1859–1865.
(54) Lee, J.; Cheng, X.; Swails, J. M.; Yeom, M. S.; Eastman, P. K.; Lemkul, J. A.; Wei, S.; Buckner, J.; Jeong, J. C.; Qi, Y. et al. CHARMM-GUI Input Generator for NAMD, GROMACS, AMBER, OpenMM, and CHARMM/OpenMM Simulations Using the CHARMM36 Additive Force Field. *J. Chem. Theory Comput.* **2016**, *12* (1), 405–413.
(55) Wu, E. L.; Cheng, X.; Jo, S.; Rui, H.; Song, K. C.; Dávila-Contreras, E. M.; Qi, Y.; Lee, J.; Monje-Galvan, V.; Venable, R. M. et al. CHARMM-GUI Membrane Builder toward Realistic Biological Membrane Simulations. *J. Comput. Chem.* **2014**, *35* (27), 1997–2004.

(56) Meyer, H. W. Pretransition-Ripples in Bilayers of Dipalmitoylphosphatidylcholine: Undulation or Periodic Segments? A Freeze-Fracture Study. *Biochim. Biophys. Acta Lipids Lipid Met.* **1996**, *1302* (2), 138–144.
(57) Pastor, R. W.; MacKerell, A. D. Development of the CHARMM Force Field for Lipids. *J. Phys. Chem. Lett.* **2011**, *2* (13), 1526–1532.
(58) Klauda, J. B.; Venable, R. M.; Freites, J. A.; O'Connor, J. W.; Tobias, D. J.; Mondragon-Ramirez, C.; Vorobyov, I.; MacKerell, A. D.; Pastor, R. W. Update of the CHARMM All-Atom Additive Force Field for Lipids: Validation on Six Lipid Types. *J. Phys. Chem. B* **2010**, *114* (23), 7830–7843.
(59) Abraham, M. J.; Murtola, T.; Schulz, R.; Páll, S.; Smith, J. C.; Hess, B.; Lindahl, E. GROMACS: High Performance Molecular Simulations through Multi-Level Parallelism from Laptops to Supercomputers. *SoftwareX* **2015**, *1*, 19–25.
(60) Braun, E.; Gilmer, J.; Mayes, H. B.; Mobley, D. L.; Monroe, J. I.; Prasad, S.; Zuckerman, D. M. Best Practices for Foundations in Molecular Simulations [Article v1.0]. *Living J. Comp. Mol. Sci.* **2018**, *1* (1), 5957.
(61) Smith, D. J.; Klauda, J. B.; Sodt, A. J. Simulation Best Practices for Lipid Membranes [Article v1.0]. *Living J. Comp. Mol. Sci.* **2018**, *1* (1), 5966.
(62) Lemkul, J. From Proteins to Perturbed Hamiltonians: A Suite of Tutorials for the GROMACS-2018 Molecular Simulation Package [Article v1.0]. *Living J. Comp. Mol. Sci.* **2018**, *1* (1), 5068.
(63) Darden, T.; York, D.; Pedersen, L. Particle Mesh Ewald: An N.Log(N) Method for Ewald Sums in Large Systems. *J. Chem. Phys.* **1993**, *98* (12), 10089–10092.
(64) Hess, B. P-LINCS: A Parallel Linear Constraint Solver for Molecular Simulation. *J. Chem. Theory. Comput.* **2008**, *4* (1), 116–122.
(65) Bussi, G.; Donadio, D.; Parrinello, M. Canonical Sampling through Velocity Rescaling. *The J. Chem. Phys.* **2007**, *126* (1), 014101.
(66) Parrinello, M.; Rahman, A. Polymorphic Transitions in Single Crystals: A New Molecular Dynamics Method. *J. Appl. Phys.* **1981**, *52* (12), 7182–7190.
(67) Alavi, S.; Thompson, D. L. Molecular Dynamics Studies of Melting and Some Liquid-State Properties of 1-Ethyl-3-Methylimidazolium Hexafluorophosphate [Emim][PF6]. *J. Chem. Phys.* **2005**, *122* (15), 154704.
(68) Zhang, Y.; Maginn, E. J. A Comparison of Methods for Melting Point Calculation Using Molecular Dynamics Simulations. *J. Chem. Phys.* **2012**, *136* (14), 144116.
(69) Wassenaar, T. A.; Ingólfsson, H. I.; Böckmann, R. A.; Tieleman, D. P.; Marrink, S. J. Computational Lipidomics with Insane: A Versatile Tool for Generating Custom Membranes for Molecular Simulations. *J. Chem. Theory. Comput.* **2015**, *11* (5), 2144–2155.
(70) de Jong, D. H.; Baoukina, S.; Ingólfsson, H. I.; Marrink, S. J. Martini Straight: Boosting Performance Using a Shorter Cutoff and GPUs. *Comput. Phys. Commun.* **2016**, *199*, 1–7.
(71) Tironi, I. G.; Sperb, R.; Smith, P. E.; van Gunsteren, W. F. A Generalized Reaction Field Method for Molecular Dynamics Simulations. *J. Chem. Phys.* **1995**, *102* (13), 5451–5459.
(72) Humphrey, W.; Dalke, A.; Schulten, K. VMD: Visual Molecular Dynamics. *J. Mol. Graph.* **1996**, *14* (1), 33–38.
(73) Guixà-González, R.; Rodriguez-Espigares, I.; Ramírez-Anguita, J. M.; Carrió-Gaspar, P.; Martinez-Seara, H.; Giorgino, T.; Selent, J. MEMBPLUGIN: Studying Membrane Complexity in VMD. *Bioinformatics* **2014**, *30* (10), 1478–1480.
(74) Varadarajan, V.; Desikan, R.; Ayappa, K. G. Assessing the Extent of the Structural and Dynamic Modulation of Membrane Lipids Due to Pore Forming Toxins: Insights from Molecular Dynamics Simulations. *Soft Matter* **2020**, *16* (20), 4840–4857.
(75) Koynova, R.; Caffrey, M. Phases and Phase Transitions of the Hydrated Phosphatidylethanolamines. *Chem. Phys. Lipids* **1994**, *69* (1), 1–34.
(76) Nagai, T.; Okamoto, Y. Replica-Exchange Molecular Dynamics Simulation of a Lipid Bilayer System with a Coarse-Grained Model. *Mol. Sim.* **2012**, *38* (5), 437–441.

(77) Manna, M.; Nieminen, T.; Vattulainen, I. Understanding the Role of Lipids in Signaling Through Atomistic and Multiscale Simulations of Cell Membranes. *Annu. Rev. Biophys.* **2019**, *48* (1), 421–439.
(78) Jarin, Z.; Newhouse, J.; Voth, G. A. Coarse-Grained Force Fields from the Perspective of Statistical Mechanics: Better Understanding of the Origins of a MARTINI Hangover. *J. Chem. Theory Comput.* **2021**, *17* (2), 1170–1180.

Supporting information

Evaluating Coarse-Grained MARTINI Force-Fields for Capturing the Ripple Phase of Lipid Membranes

***Pradyumn Sharma*[1,‡], *Rajat Desikan*[1,‡,†], *K. Ganapathy Ayappa*[1,2,*]**

[1]Department of Chemical Engineering, Indian Institute of Science, Bengaluru, India

[2]Centre for BioSystems Science and Engineering, Indian Institute of Science, Bengaluru, India

[‡]Co-first authors

[†]Present address: Certara QSP, Certara UK Limited, Sheffield, UK

*Corresponding author: K. Ganapathy Ayappa; E-mail: ayappa@iisc.ac.in

Author contributions

Conceptualization: R.D.; Data curation: P.S.; Formal analysis: R.D. and P.S.; Funding acquisition: K.G.A.; Investigation: P.S. and R.D.; Methodology: R.D. and P.S.; Project administration: P.S. and R.D.; Resources: P.S., R.D. and K.G.A.; Software (simulations, analysis code): P.S. and R.D.; Supervision: K.G.A.; Validation: P.S., R.D. and K.G.A.; Visualization: P.S. and R.D.; Writing – original draft: R.D. and P.S.; Writing – review & editing: R.D., P.S. and K.G.A.

All authors have given approval to the final version of the manuscript.

[‡]These authors (P.S. and R.D.) contributed equally.

Supporting figures

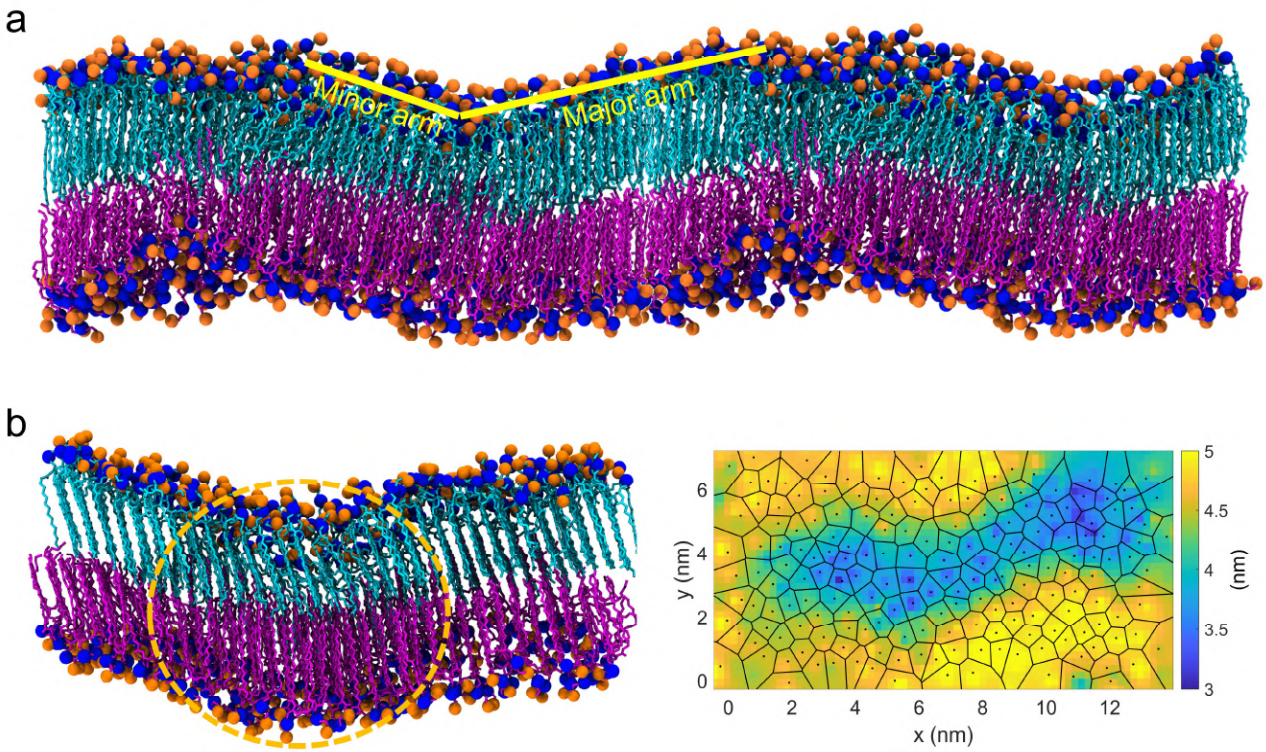

Figure S1. An independent all-atom MD replicate reproduces the ripple phase. (a) MD snapshot at time point IV from Figure 1*a* is periodically repeated along the x-axis, and the major and minor arms of the ripple in the upper leaflet are visually annotated for clarity. **(b)** Final snapshot (time point IV in Figure 1) and corresponding Voronoi-thickness diagram from the independent simulated cooling replicate, using the same MD protocol as for the replicate in Figure 1, shows robust reproduction of the tilted ripple phase from all-atom simulations.

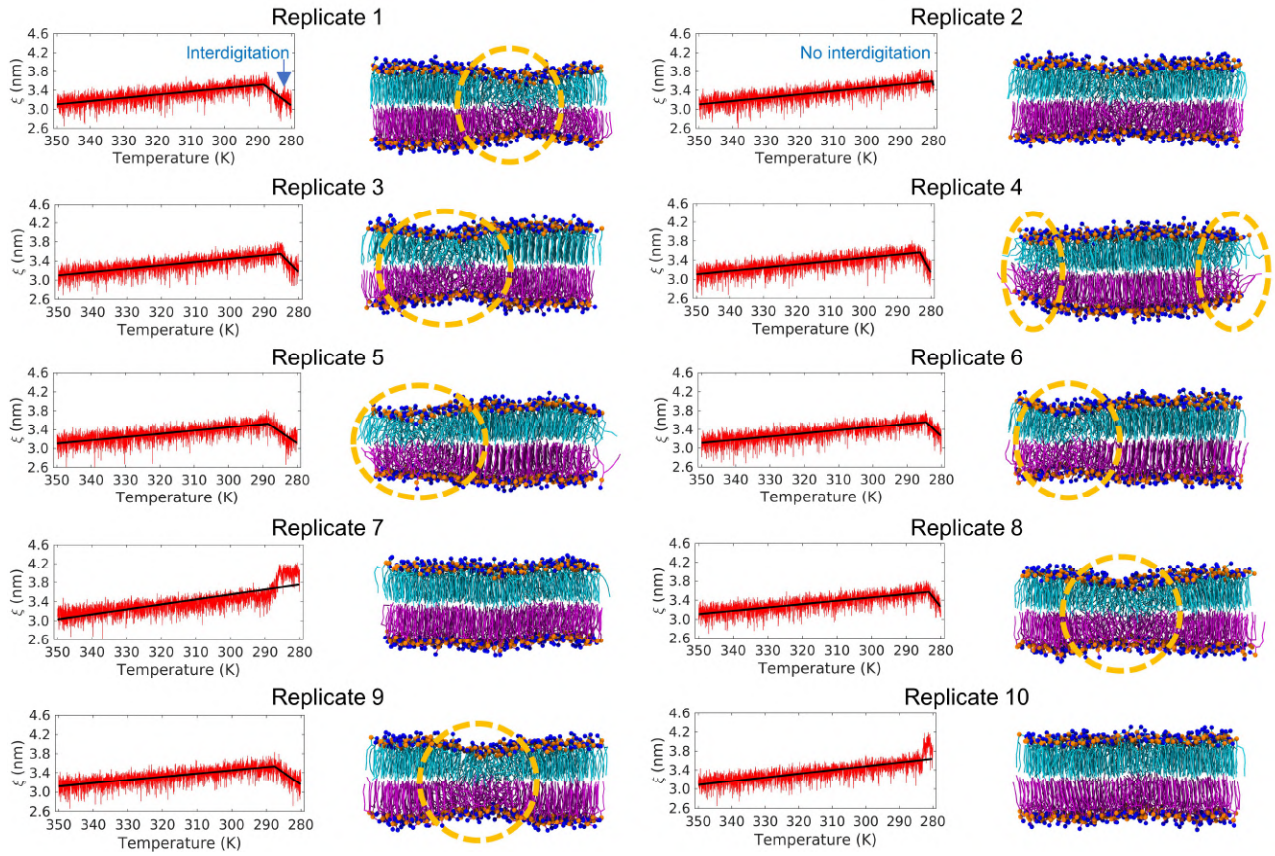

Figure S2. Summary of 10 independent cooling MD replicates with the MARTINI2n FF. Temporal evolution of the minimum inter-leaflet P-P distance (ξ), a measure of the extent of interdigitation (Figure 1*b*; $m_2 < 0$ – interdigitation, and $m_2 > 0$ – no interdigitation (Methods, Eq. 1), are highlighted in replicates 1 and 2, respectively). Final snapshots corresponding to time point III at the end of cooling simulations with MARTINI2n DPPC membranes are shown for all the 10 independent MD replicates. The interdigitated domains in replicates which exhibit ripple-like structures are marked with yellow dashed circles.

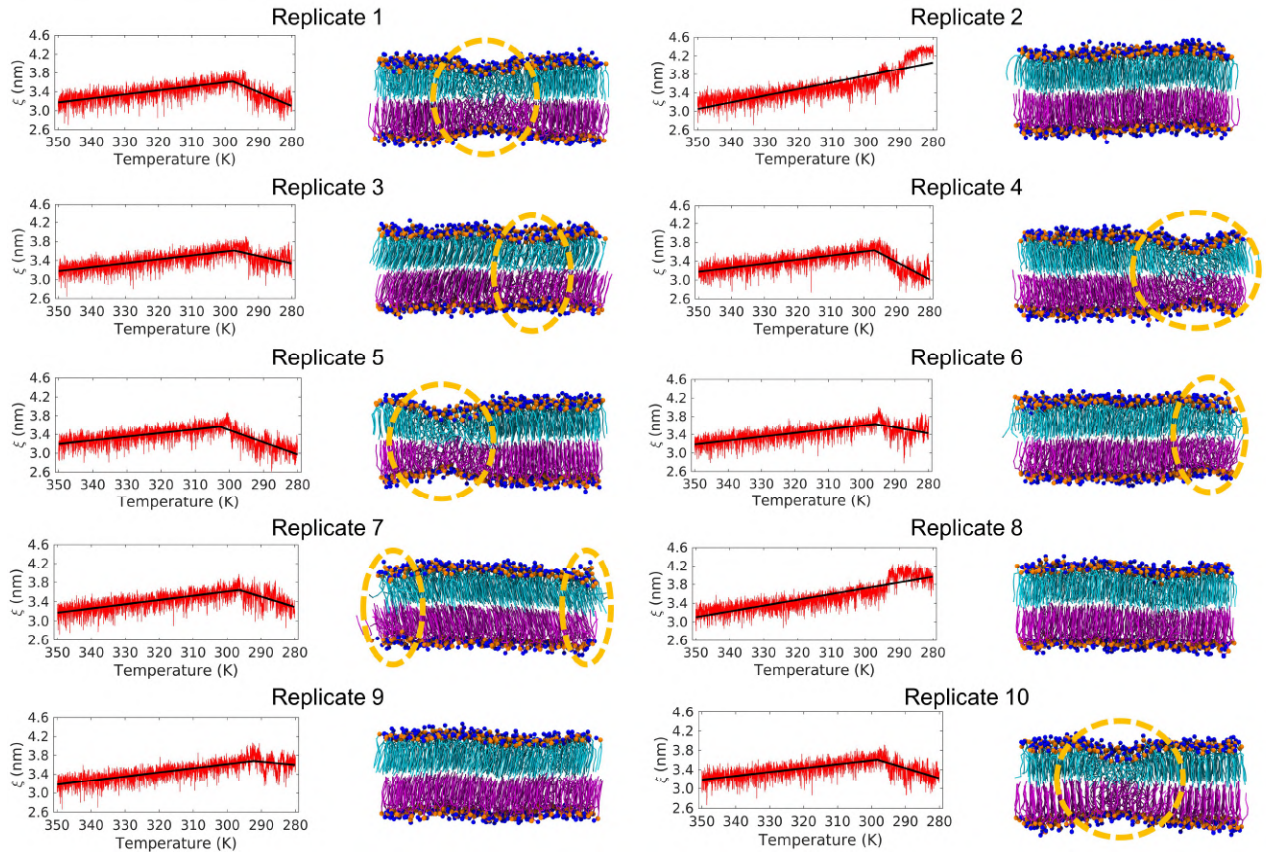

Figure S3. Summary of 10 independent cooling MD replicates with the MARTINI2On FF. Same as Figure S2, but with the MARTINI2On FF variant.

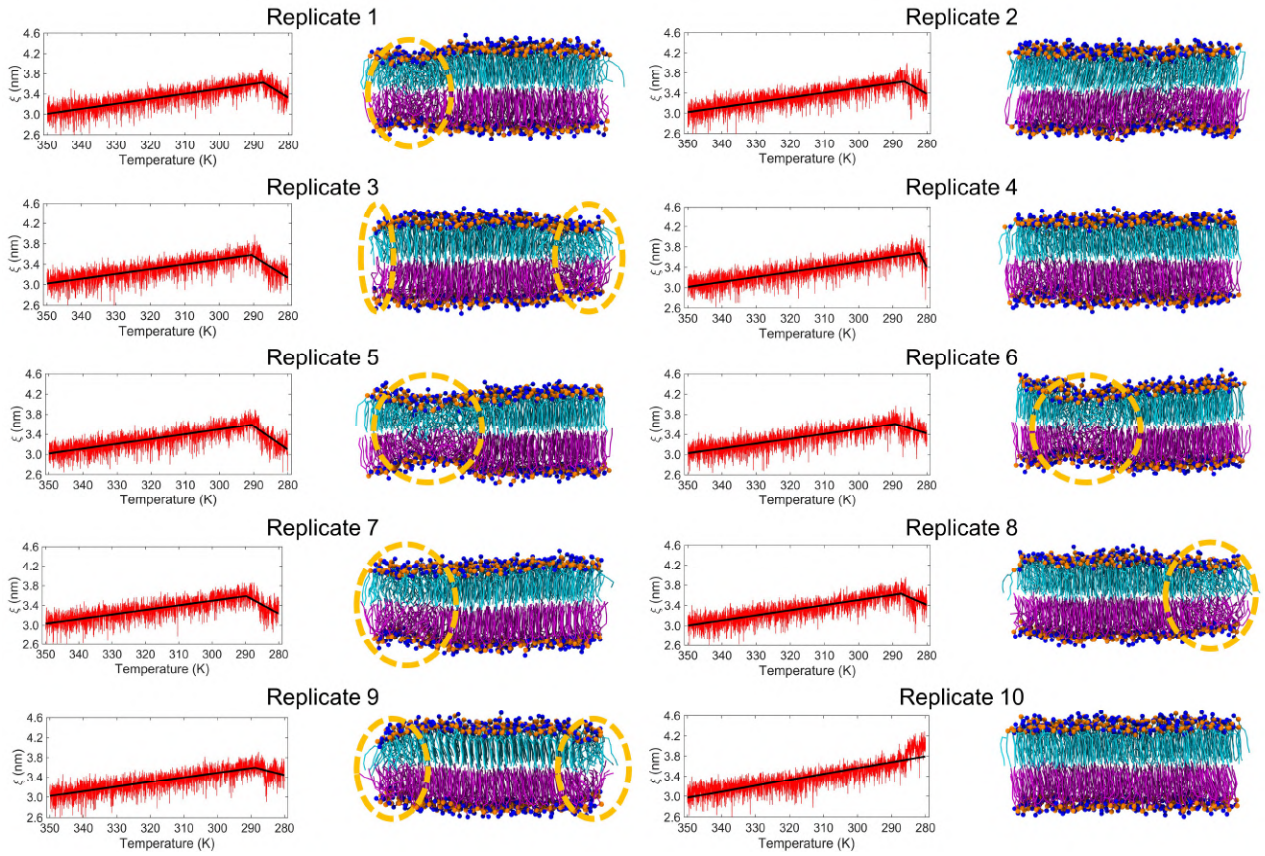

Figure S4. Summary of 10 independent cooling MD replicates with the MARTINI3a FF. Same as Figure S2, but with the MARTINI3a FF variant. Note that while the ξ trends for replicates 2 and 4 appear to indicate the onset of ripple formation, it can be inferred from visual inspection that this is due to very few interdigitating lipids and not due to the formation of a ripple-like domain. Hence, these replicates were not counted as ripple-like states.

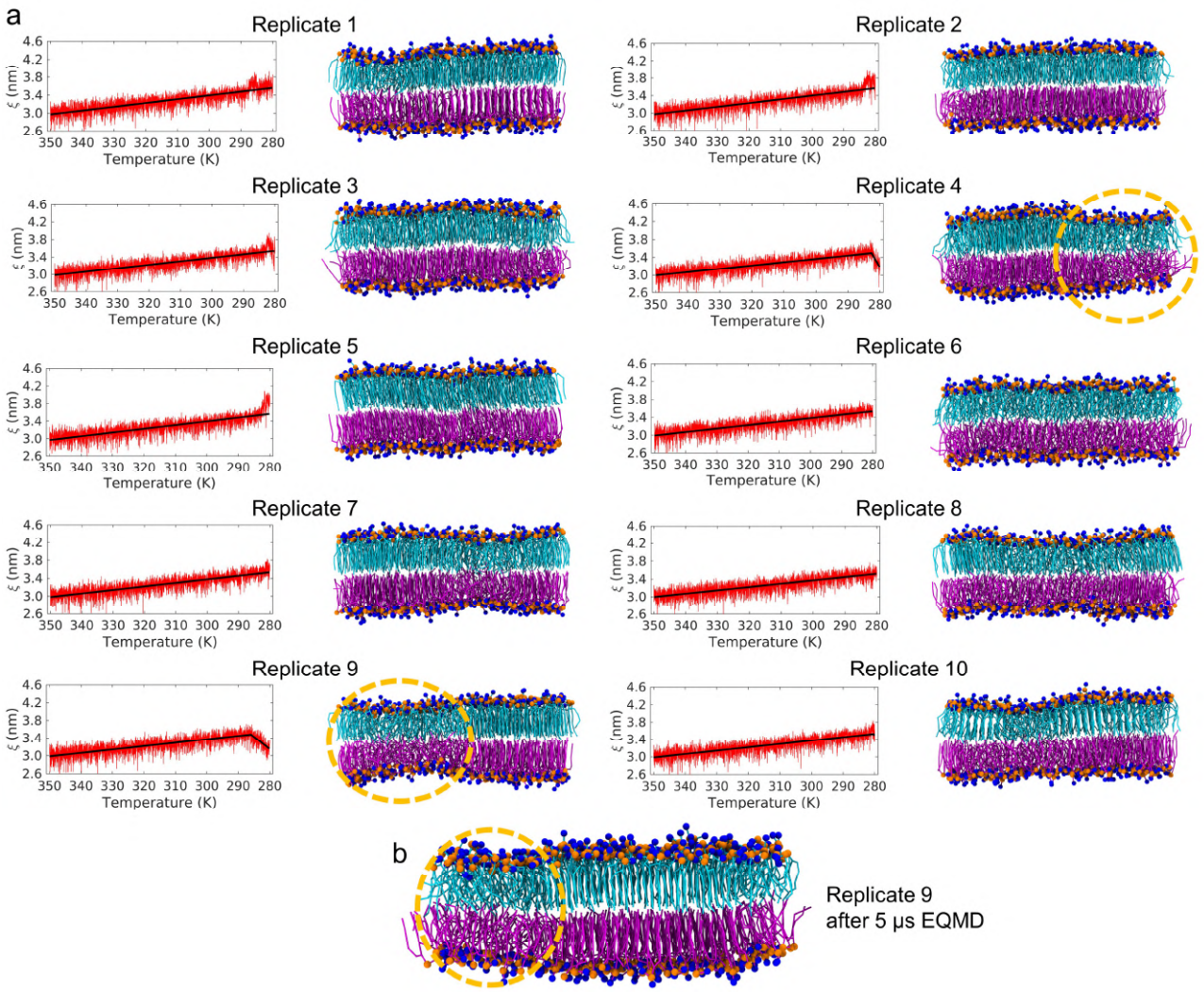

Figure S5. Summary of 10 independent cooling MD replicates with the MARTINI3b FF. (a) Same as Figure S2, but with the MARTINI3b FF variant. **(b)** Replicate 9 was further subjected to 5 μs EQMD to confirm that the ripple-like domains were stable at this timescale.

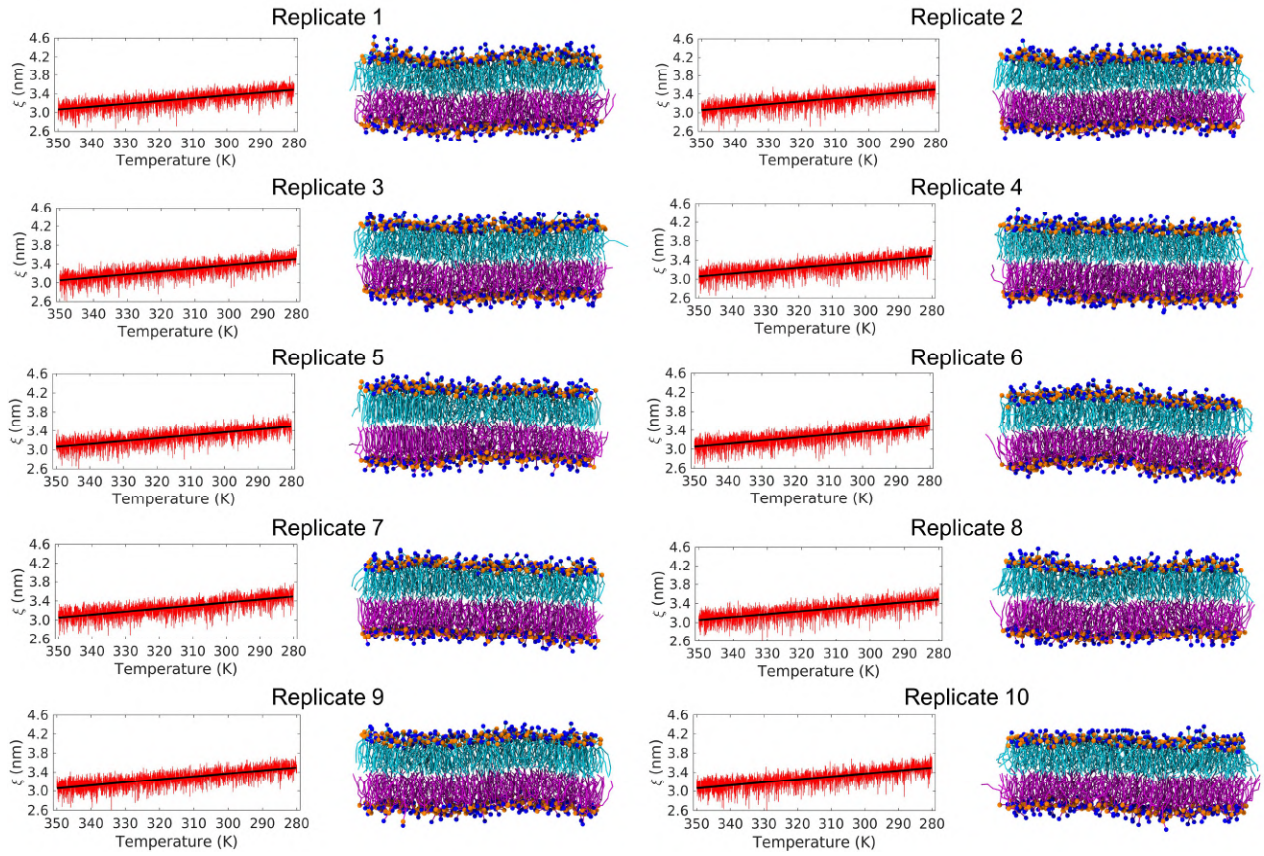

Figure S6. Summary of 10 independent cooling MD replicates with the MARTINI2p FF. Same as Figure S2, but with the MARTINI2p FF variant. Note that while none of the *ξ* plots show ripple-like domain formation during the cooling phase, replicate 5 formed shallow interdigitated ripple-like domains during the 5 μs EQMD (Figure 2*f*).

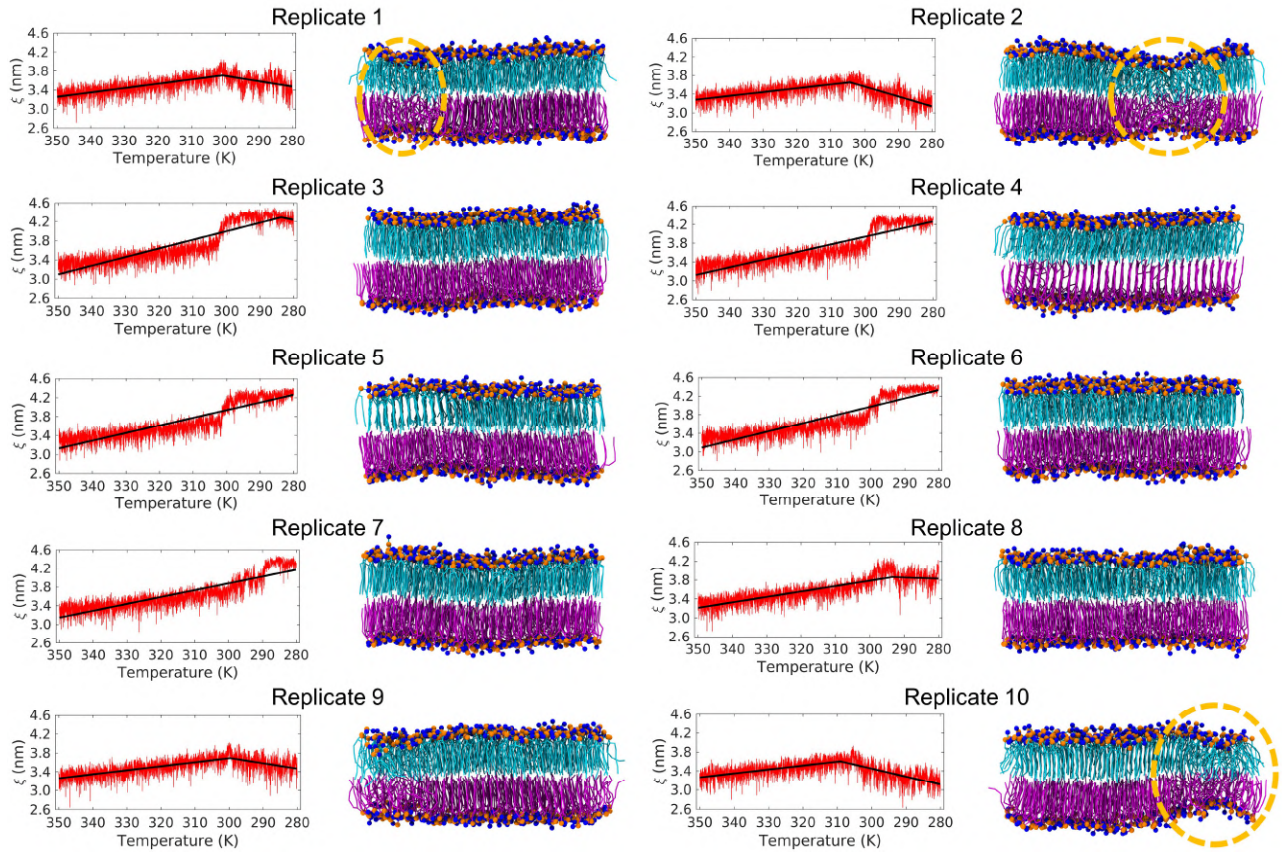

Figure S7. Summary of 10 independent cooling MD replicates with the MARTINI2Op FF. Same as Figure S2, but with the MARTINI2Op FF variant. In replicate 9, while we observed a ξ trend similar to ripple-like domain formation, visual inspection yielded no interdigitated domains, and hence this replicate was not considered as a ripple-like state.

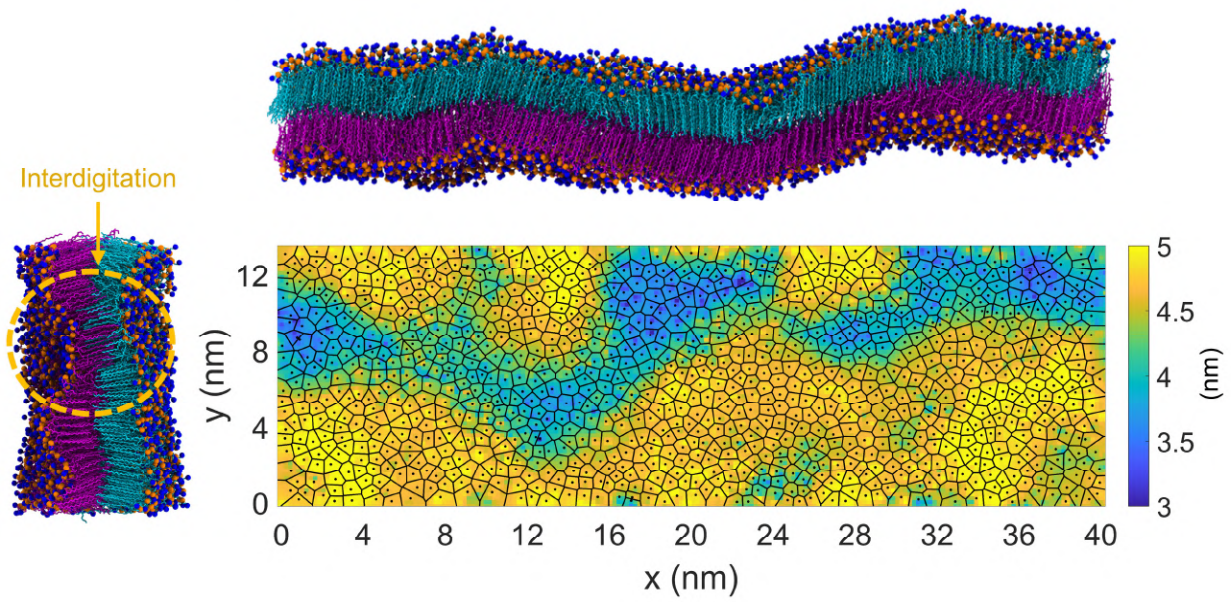

Figure S8. Independent all-atom simulation replicate also shows ripple formation in a large DPPC membrane. Similar to Figure 3, the final snapshot (front view) of a large DPPC membrane after being cooled to 290 K, and its corresponding Voronoi-thickness map, show the formation of symmetric, and asymmetric-interdigitated, ripple structures along the X-axis (shorter box dimension) and Y-axis (shorter box dimension), respectively. Note that the non-interdigitated symmetric ripple along the X-axis is indiscernible from the Voronoi-thickness map.

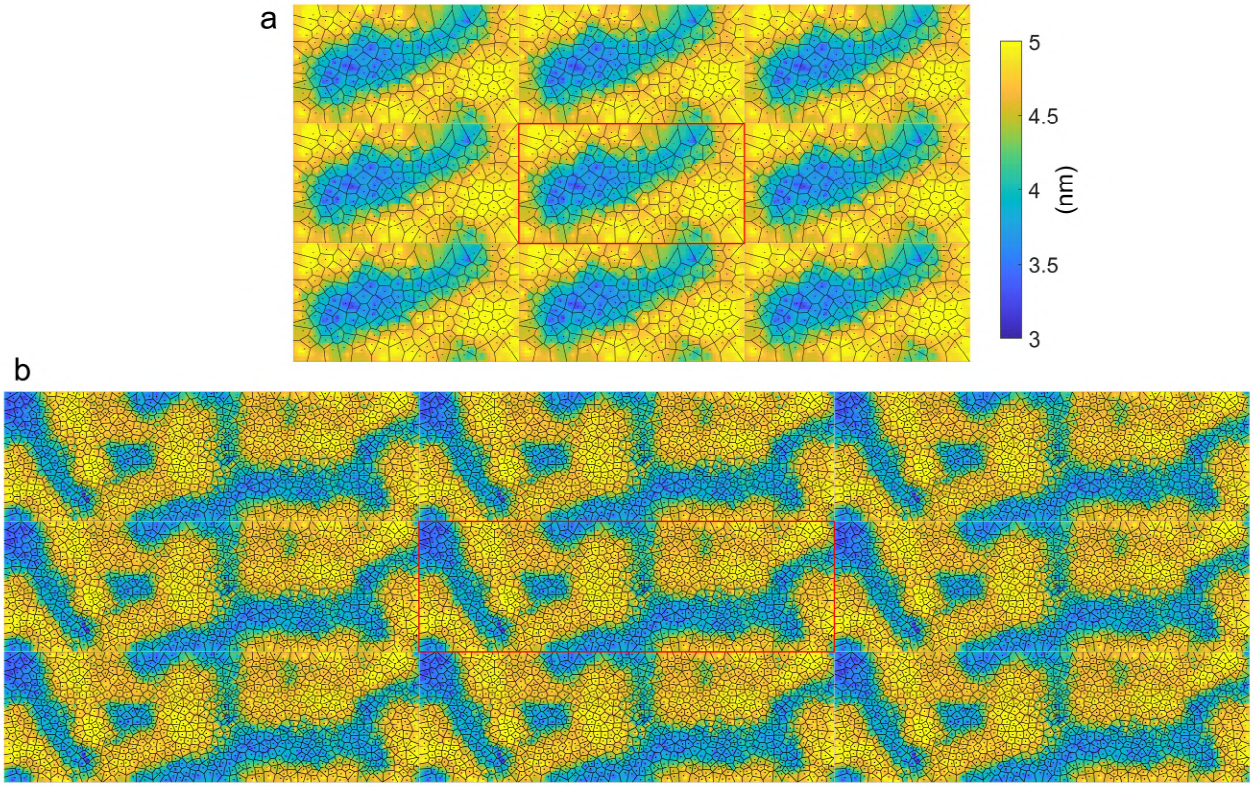

Figure S9. Periodically repeated Voronoi-thickness modulation heatmaps of atomistic DPPC membranes. Voronoi-thickness modulation heatmaps after simulated cooling of atomistic **(a)** 368-lipid (Figure 1), and **(b)** 2208-lipid (Figure 3) DPPC membranes are shown with periodic images (original simulation box in the middle shown with a red border; same thickness colorbar applies for both systems). The reticulated interdigitated domains in the larger membrane contrast with the island-like isolated domains in the smaller membrane.

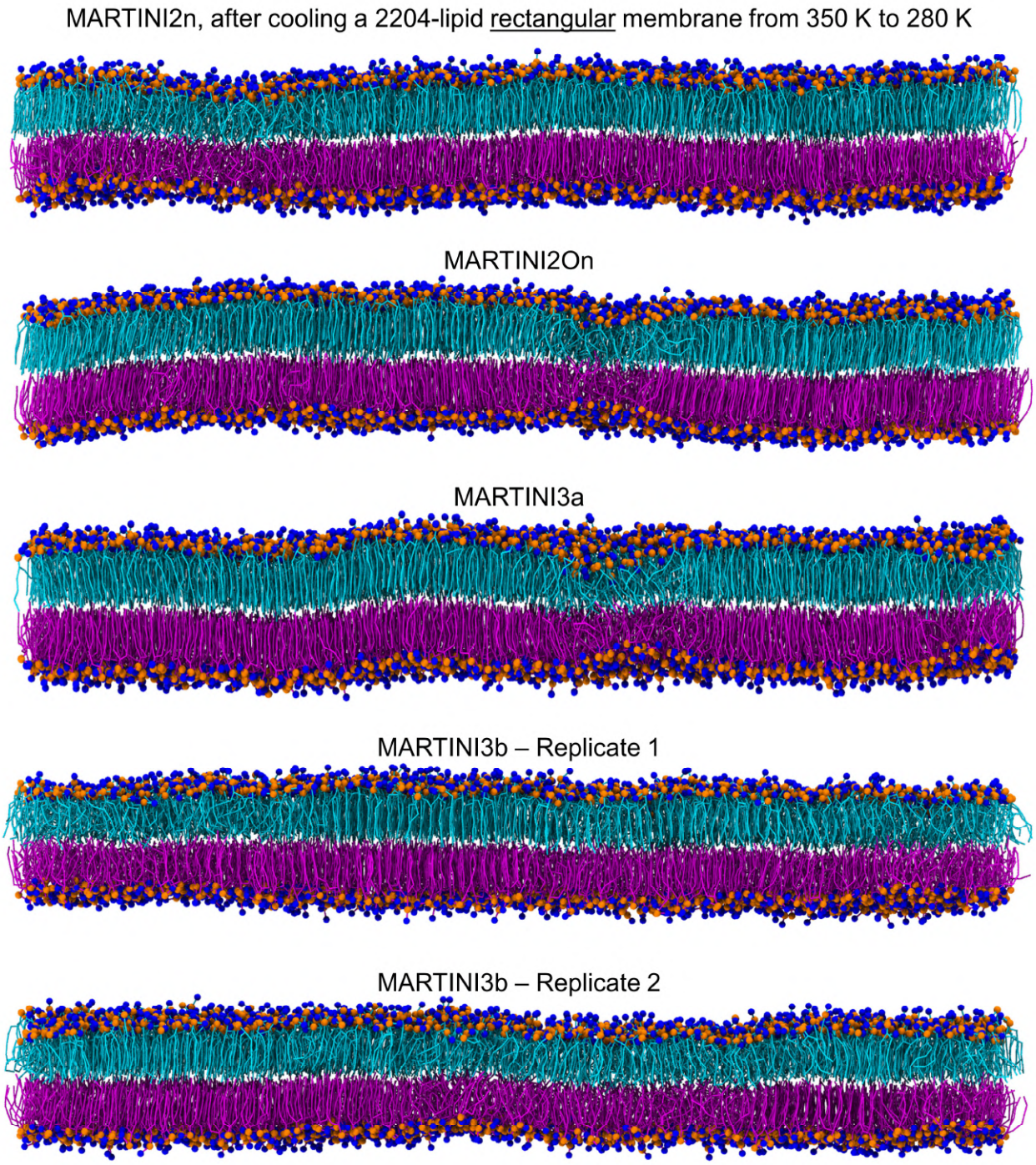

Figure S10 Independent MD replicates confirm the lack of ripple formation in large MARTINI DPPC membranes. Independent MD replicates similar to Figure 4, where large, rectangular, MARTINI2n, MARTINI2On, MARTINI3a, and MARTINI3b DPPC membranes, initially pre-equilibrated in the fluid phase at 350 K, exhibited direct transformation into the straight gel phase upon cooling to 280 K without forming either interdigitated or symmetric ripple-like structures (unlike the behaviour for smaller MARTINI membranes in Figure 2). Note: these

membranes were not subject to further EQMD after cooling, and thus a few minor domains remain in the L_α state. These are expected to disappear upon further equilibration.

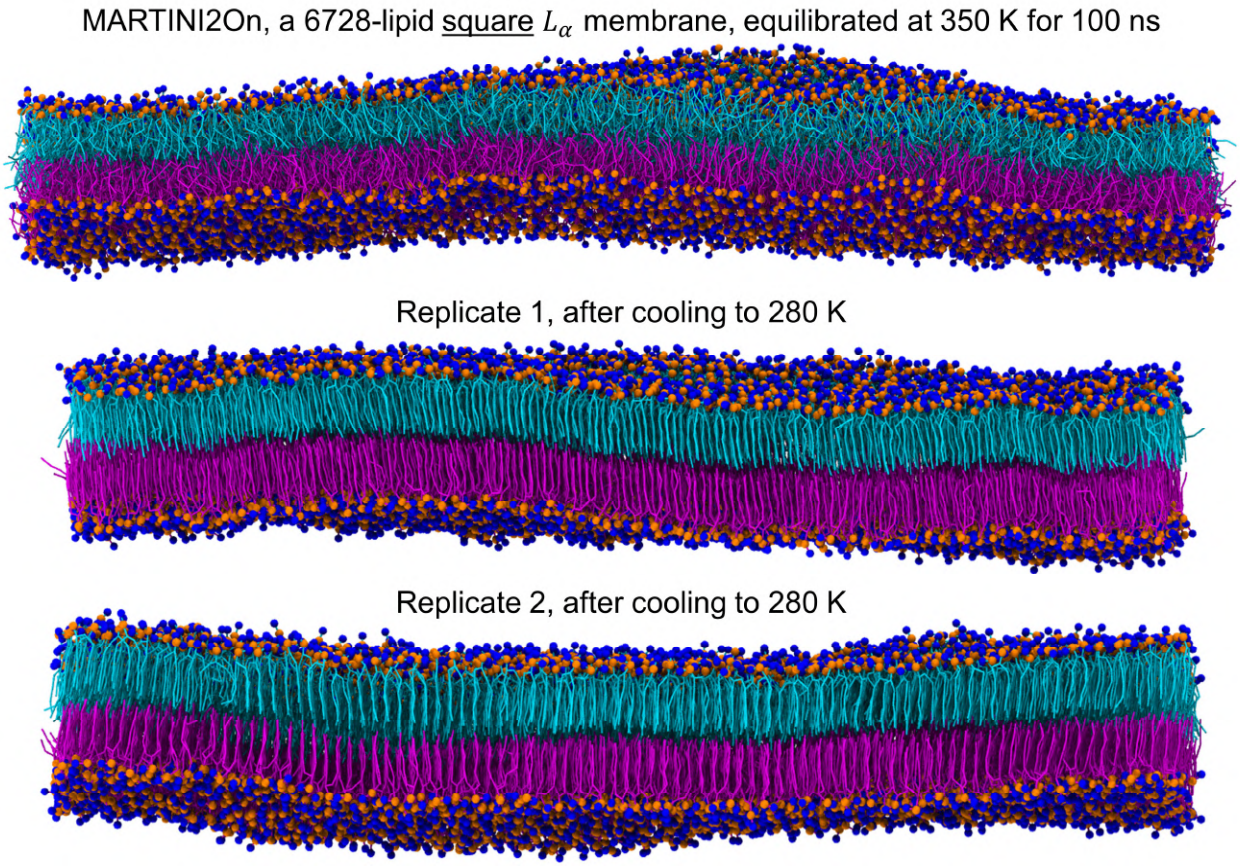

Figure S11 Large square MARTINI DPPC membranes also exhibit a lack of ripple formation. The influence of membrane geometry on ripple formation was also tested by cooling two large, square, MARTINI2On membrane replicates, from 350 K to 280 K. Similar to the rectangular membrane patches in Figure S10, both square membrane replicates directly froze into the gel phase without forming ripple membranes.

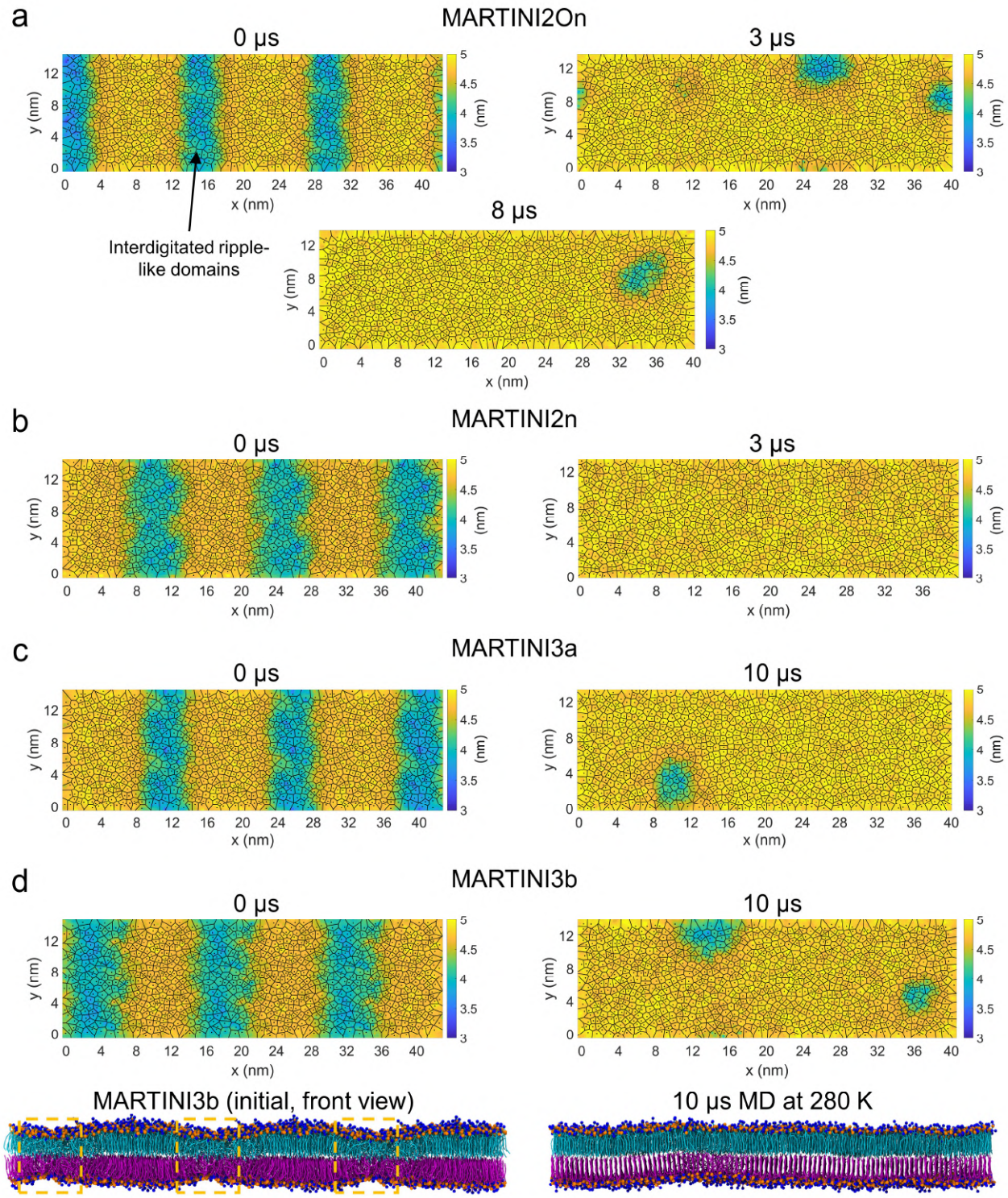

Figure S12. Voronoi-thickness maps from MD of large MARTINI membranes. Voronoi-thickness map from constant temperature MD of large **(a)** MARTINI2On, **(b)** MARTINI2n, **(c)** MARTINI3a, and **(d)** MARTINI3b membranes at 280 K, corresponding to MD snapshots in Figure 5 (snapshots for MARTINI3b shown here). Simulations starting with a periodic ripple-like configuration (0 μs), shows progressive loss of the interdigitated ripple-like domains and formation

of the gel phase by 8 μs and 10 μs for the MARTINI2On and MARTINI3a/b membranes, respectively. Notably, the MARTINI2n membrane shows complete loss of interdigitation by 3 μs. While the blue regions at the initial time points (0 μs) correspond to interdigitated domains, they could correspond to either metastable interdigitated (continuously decreasing), or non-interdigitated but partially melted domains, at the final time points. This distinction can be made by simultaneously comparing the MD snapshots (Figure 5 for MARTINI2On, MARTINI2n, MARTINI3a, and above for MARTINI3b) with the Voronoi-thickness maps above.

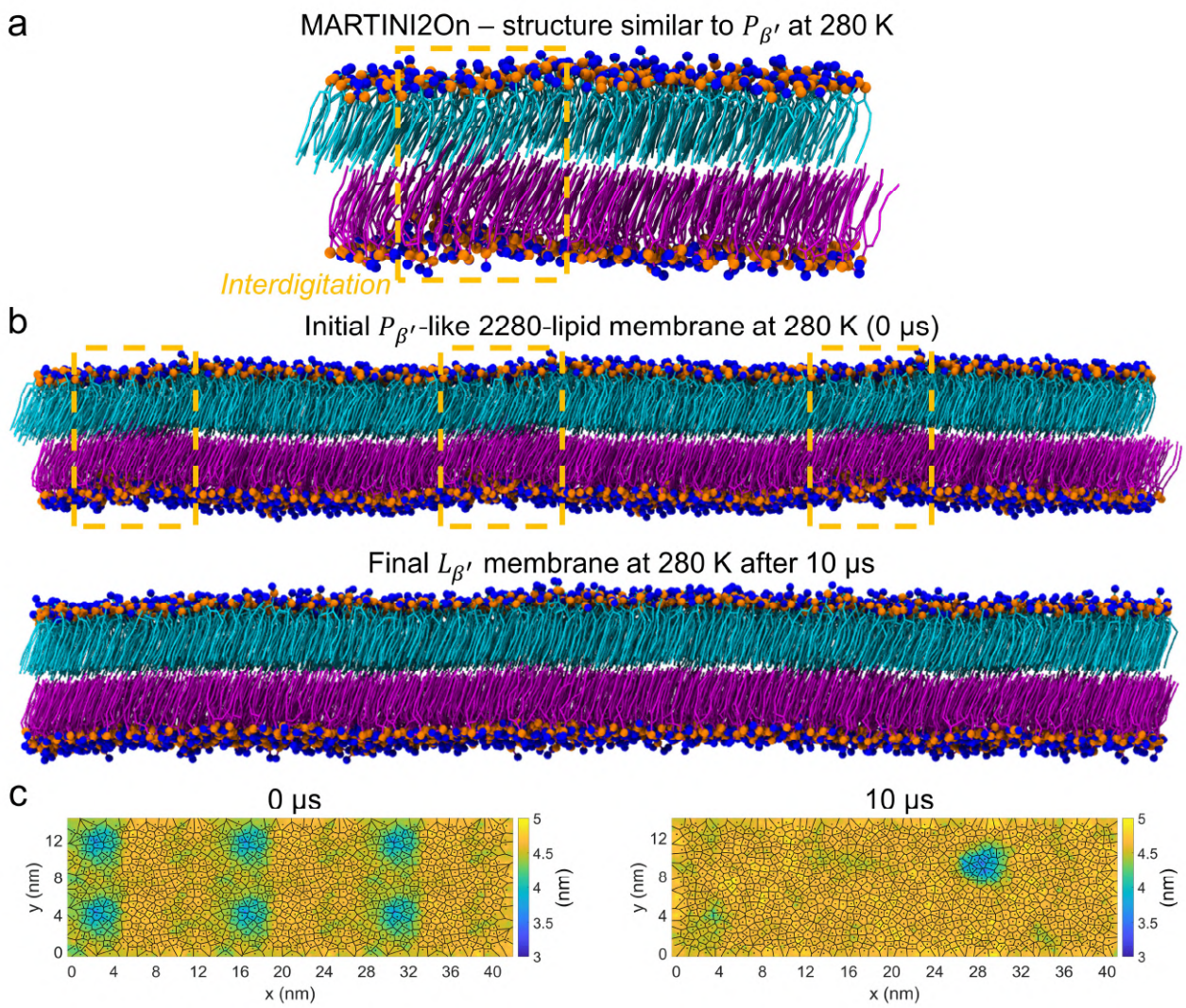

Figure S13. Tilted ripple-like state of MARTINI2On membranes is also a finite size artefact. Simulated cooling of replicate 3 with the MARTINI2On FF (from Figure S3) showed the formation of an interdigitated domain in an otherwise $L_{\beta'}$ membrane at 280 K. This structure was enhanced upon performing constant temperature MD for 5000 ns: final snapshot shown in **(a)**. **(b)** To explore whether this was a finite size effect or a true ripple phase, the smaller membrane was replicated 6x across periodic boundaries to create a larger membrane with repeated ripple-like domains (snapshot at 0 μs), similar to Figure 5*a*. After 10 μs constant temperature MD, the interdigitated ripple-like regions were greatly diminished, thus confirming that the ripple-like state in (a) was indeed a finite size artefact. **(c)** Voronoi-thickness maps pertaining to MD snapshots in (b), where regions of lower thickness in blue indicate the ripple-like domains.